JPL D xxxx
EOS MLS DRL 601 (part 6)
ATBD-MLS-06

Earth Observing System (EOS)

Microwave Limb Sounder (MLS)

EOS MLS Level 3 Algorithms Theoretical Basis

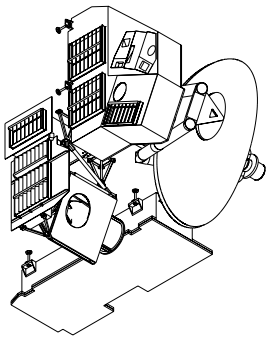

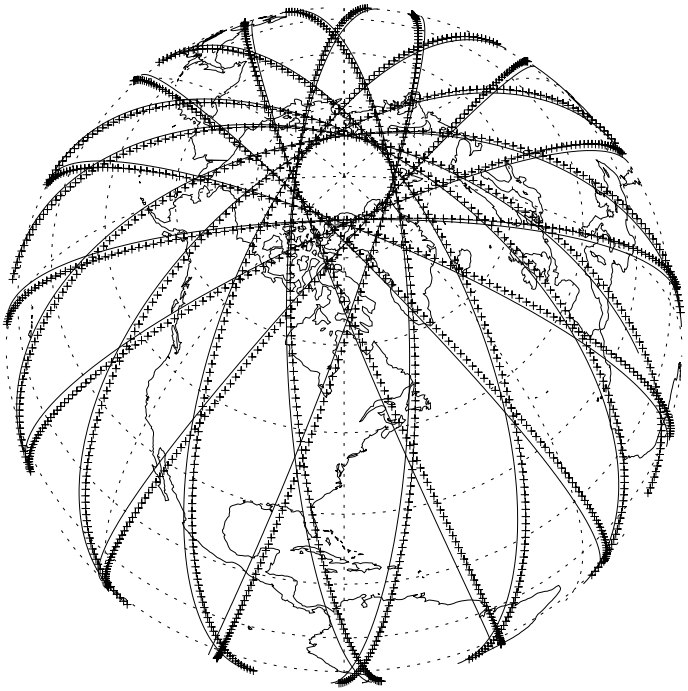

Note: Plan to overlay reconstructed map on this after we get results from V0.5 software.

Yibo Jiang

Version 0.5 (draft)

March 24, 2000

Jet Propulsion Laboratory
California Institute of Technology
Pasadena, California 91109-8099

Release Record

Version	date released	comments
0.5	24 March, 2000	initial release for MLS internal review

TABLE OF CONTENTS

1. Introduction

1.1 The EOS MLS Experiment

EOS MLS is an experiment on the NASA EOS CHEMISTRY (CHEM) satellite mission currently scheduled for launch in December 2002, with an operational period extending 5 years or longer after launch. The overall objective of EOS MLS is to help provide measurements and information that are needed for improving understanding of global change in Earth's stratosphere, upper troposphere and mesosphere

EOS MLS is a greatly enhanced version of the Upper Atmosphere Research Satellite (UARS) MLS experiment. It provides measurements of several stratospheric chemical species (O_3, H_2O, OH, HO_2, CO, HCN, N_2O, HNO_3, HCl, HOCl, ClO, BrO, volcanically-injected SO_2), temperature and geopotential height. It measures upper tropospheric H_2O, temperature, O_3, CO, HCN, N_2O, HCl (all of which can be made even in the presence of ice clouds), cloud ice and geopotential height. Mesospheric temperature, H_2O, OH, HO_2, O_3, HCl, CO and geopotential height are measured to provide information on this higher region of Earth's atmosphere.

The EOS CHEM orbit is sun-synchronous at 705 km altitude with 98^o inclination and 1:45 p.m. ascending equator-crossing time. MLS performs observations with the instrument fields-of-view scanning the limb *in the orbit plane* to provide 82^o N to 82^o S latitude coverage on each orbit.

The limb scans for nominal operation are synchronized to the orbit (using the node-crossing signal from the spacecraft), with the number of scans per orbit an integer multiple of 4, and phased such that limb scan locations occur over the equator. This gives the same latitude sampling in the northern and southern hemispheres, and on the ascending and descending portions of the orbit. MLS nominal operations have 240 limb scans per orbit to give 1.5^o (165 km) along-track separation between adjacent limb scans; this separation is well-matched to the along-track resolution expected for upper tropospheric water vapor measurements. Figure 1-1 shows the locations of measurements with this scan pattern for one 24-hour period.

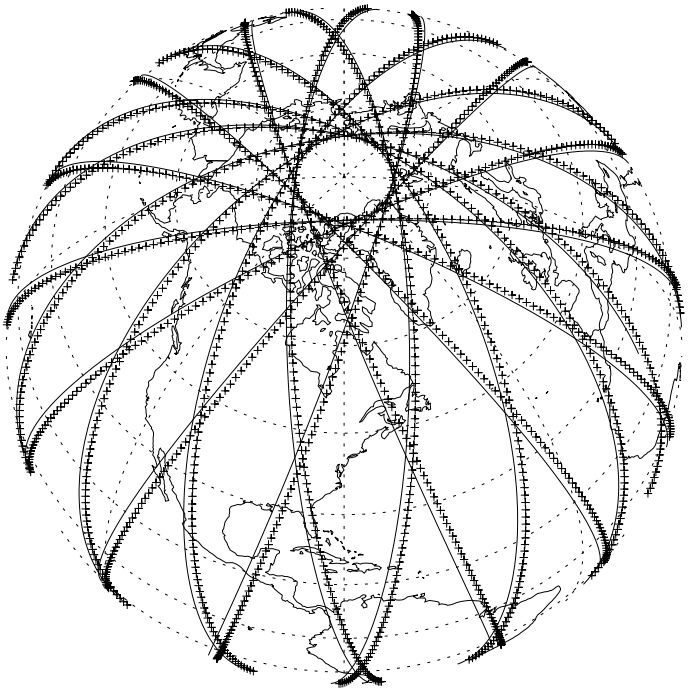

Figure 1-1. EOS MLS measurement locations for a 24 hour period. Each cross gives the location of the tangent points for individual limb scans. The continuous line is the suborbital track, which is slightly displaced from the tangent points because of Earth's rotation during the time in which the satellite moves forward to the tangent point latitude. The ascending portions of the orbit are those with the southeast-northwest tilt. Daily coverage at high latitudes in the Southern Hemisphere is analogous to that of the Northern Hemisphere shown here. R.R. Lay prepared this figure.

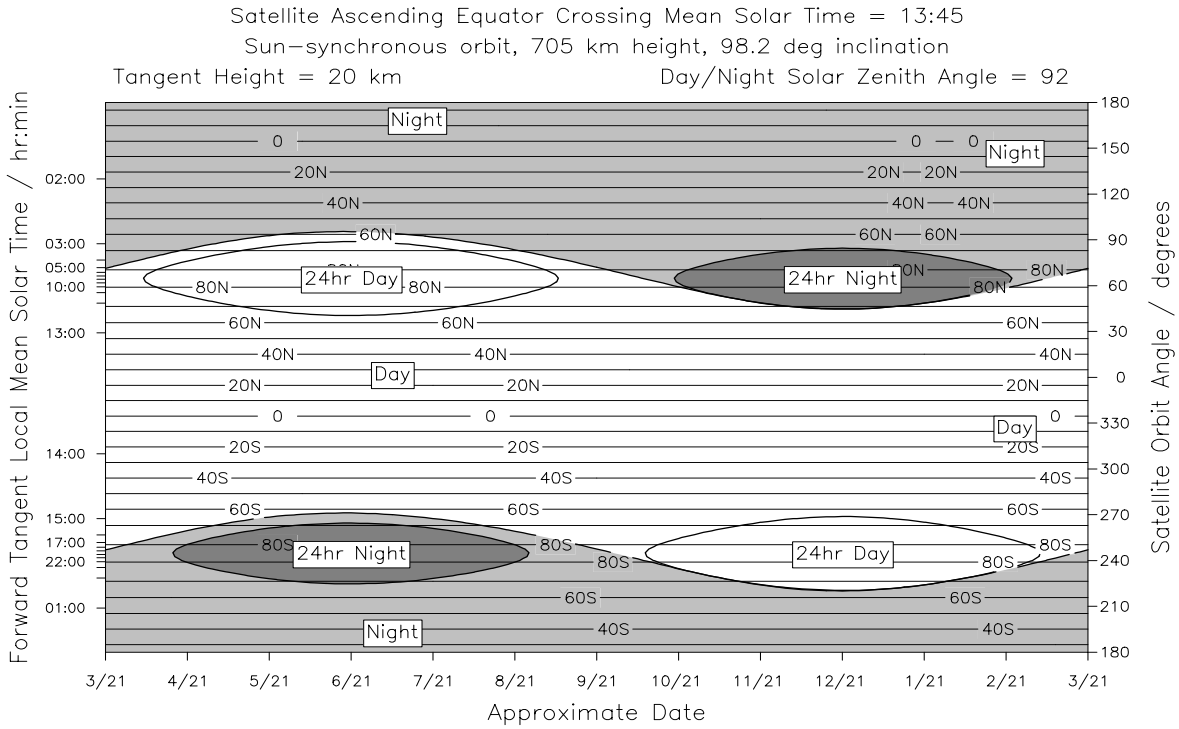

Figure 1-2. Variation, over an annual cycle, of the latitude range where MLS measurements are in day and in night. The horizontal axis gives the approximate date. The right hand vertical axis gives the orbit angle (defined as zero when the satellite is over the equator); the left hand vertical axis gives the corresponding local mean solar time at the (forward) tangent point of MLS observations. Horizontal lines give the latitude of the MLS tangent point, and the day-night boundary is defined as 92^o local solar zenith angle. M.J. Filipiak prepared this figure.

As the EOS CHEM orbit is sun-synchronous (i.e., the orbit plane has a constant orientation relative to the Earth-Sun line), MLS observations at a given latitude on either the ascending (north-going) or descending (south-going) portions of the orbit have the same local solar time throughout the mission as indicated in Figure 1-2. The local solar zenith angle at a given latitude, and the boundaries between the day and night portions of the orbit, vary around an annual cycle as also shown in Figure 1-2.

Data from EOS MLS are routinely processed to various 'Levels' as follow

- 'Level 1' data are calibrated radiances and engineering data from the instrument, with ancillary data such as time, location, satellite attitude, etc. The Level 1B data are in daily files, each covering 0-24 hours GMT. Jarnot [1999] gives the theoretical basis for the EOS MLS Level 1 data processing algorithms.
- Level 2' data are vertical profiles of geophysical parameters (and their uncertainties) retrieved at the nominal limb scan locations, along with ancillary and diagnostic data such as time, location, local solar time, solar zenith angle, etc. The Level 2 data are in daily files, each covering 0-24 hours GMT. Livesey and Wu [1999] gives the theoretical basis for the retrieval processes algorithms used in EOS MLS Level 2 data processing.
- Level 3' data are 'gridded' products that include:
  (1) daily global maps for measurements having sufficiently high signal to noise,
  (2) monthly global maps for all Level 2 geophysical products,
  (3) daily zonal means for all Level 2 geophysical products, and
  (4) monthly zonal means for all Level 2 geophysical products.

The EOS MLS 'Overview' document [*Waters*, 1999] gives additional overall information on the EOS MLS experiment.

1.2 The purpose of this document

The purpose of this document is to give the theoretical basis for algorithms used to produce all Level 3 products for those EOS MLS measurements that have sufficiently high signal-to-noise to produce useful daily maps. These products are listed in section 1.3, and will be produced using only the MLS Level 2 data files as inputs.

Algorithms for producing the MLS Level 3 products from the other MLS measurements, the 'noisy' measurements, are described in Livesey and Wu [1999]. Those Level 3 products are produced directly from the MLS Level 1 data

It should be noted that, although the algorithms described here are developed for those MLS measurements with sufficiently high signal-to-noise, they can also be used with *any* MLS Level 2 file as input. This provides needed flexibility for producing daily maps for MLS measurements whose signal-to-noise may be better than now expected. It also provides cross-checking of the zonal mean and global maps to be routinely produced using the other algorithms mentioned above for 'noisy' measurements.

1.3 EOS MLS data products for which this document applies

1.3.1 Level 3 daily map products

Table 1-1 gives the currently-planned EOS MLS Level 3 routine daily map products for which this document applies. Separate maps for data from the ascending and descending portions of the orbit will be made for the diurnally-varying species ClO, OH, and O_3 at higher altitudes.

Table 1-1. Level 3 Daily Map Products. The number of pressure surfaces, and volumes, assume the maximum 12 retrieval points per decade pressure, and 4-byte words for the value and precision at each grid point.

product name	units	vertical range				number of pressure surfaces	volume for one day / Megabytes
		pressure / hPa		~ height / km			
		max	min	min	max		
TEMPERATURE	K	464	0.01	0	80	56	3.35
GEOPOTENTIAL_HT	km	464	0.01	0	80	56	3.35
H2O	vmr	464	0.01	0	80	56	3.35
HNO3	vmr	100	1	15	50	24	1.43
O3	vmr	316	.316	9	55	36	2.15
O3_ascending	vmr	3.16	0.01	40	80	30	1.79
O3_descending	vmr	3.16	0.01	40	80	30	1.79
HCl	vmr	100	0.1	15	65	36	2.15
N2O	vmr	215	1	9	50	28	1.67
ClO_ascending	vmr	100	1	15	50	24	1.43
ClO_descending	vmr	100	1	15	50	24	1.43
OH_ascending	vmr	10	0.1	15	65	24	1.43
OH_descending	vmr	10	0.1	15	65	24	1.43
HCN	vmr	215	22	9	25	12	0.72
O3_STRAT_COLUMN	DU	not applicable					0.06
						total daily volume	27.55

1.3.2 Level 3 daily zonal mean products

Daily zonal mean products, using algorithms described in this document, will be produced for all the daily map products listed in Table 1-1. Current plans are to produce separate zonal means for the ascending (mostly day) and descending (mostly night) portions for each product, and the full latitudinal resolution of the corresponding Level 2 product is maintained (i.e., a zonal mean is produced for each of the nominal Level 2 latitudes), which gives better latitude resolution at high latitudes than in the Level 3 daily maps. The value and estimated precision in the daily zonal mean are included in the data files. Ancillary data included with the geophysical parameters are latitude, local solar time and local solar zenith angle.

1.3.3 Level 3 monthly map products

Level 3 monthly map products, using algorithms described in this document, will be produced for all the daily map products listed in Table 1-1. These maps represent average conditions for the month and are currently planned to be produced at the 2^o latitude by 4^o longitude grid used for the Level 3 daily maps. Separate maps for the ascending and descending sides of the orbit will be produced for diurnally-varying species, as done for the daily maps. The 'month' for these maps is defined to be the same as calendar months but, perhaps, with 'February' including 31 January and 1 March to give either 30 or 31 days for each 'EOS MLS month'.

1.3.4 Level 3 monthly zonal mean products

Level 3 monthly zonal mean products, using algorithms described in this document, will be produced for all the daily map products listed in Table 1-1. As in the daily zonal mean products, current plans are to produce separate zonal means for the ascending (mostly day) and descending (mostly night) portions of the orbit, with the full latitudinal resolution of the corresponding Level 2 product. The value and estimated precision in the monthly zonal mean are included in the data files. Ancillary data included with the geophysical parameters are latitude, and maximum and minimum values of the local solar time and local solar zenith angle for the measurement over the course of the month.

2. Overview of EOS MLS Level 3 data processing

The MLS Science Team, in consultation with other scientists who will be using MLS data, has decided to use Fast Fourier Synoptic Mapping (FFSM) techniques, initially developed by Salby [1982 a, b] to produce 'synoptic' maps as the Level 3 daily map product for measurements with sufficiently high signal-to-noise. This technique, which yields the exact transform of the data with no distortions of fast-moving waves or aliasing from high-frequency components of non-sinusoidal features, is found to be robust under reasonable conditions of randomly varying signals, sampling errors and missing data points. It has been applied previously to map data from the stratospheric sounding unit (SSU) [*Lait and Stanford*, 1988] as well as to the various measurements of UARS instruments [*Canziani et al*., 1994; *Elson and Froidevaux*, 1993; 1994; *Sassi and Salby*, 1998]. FFSM is distinguished from other approaches [e.g. *Hartmann*, 1976; *Rodgers*, 1976; *Chapman* and *McGregor*, 1978; *Hayashi*, 1983] by its sole reliance on the asynoptic measurements and their sampling in space and time. It presumes nothing of the behavior to be determined nor of the governing equations of the fields that, with correct combination of Fourier coefficients, determine the observed behavior. This procedure recovers the actual synoptic structure and evolution so long as the field property being observed is adequately sampled [*Salby and Hayashi*, 1985]. The current plan is for a map output grid of 4^o longitude by 2^o latitude (between 82 N and 82 S), and with the daily maps produced for a time corresponding to noon GMT.

Since at least several days of measurements are required - using this technique - to produce a map for a single day, the MLS Science Team has decided to do the Level 3 processing on a monthly basis. This allows all the Level 3 products (including monthly maps and zonal means) to be produced during the same processing step. 'Quick-look' algorithms will be developed, whose description is not within the scope of this document, for use on the MLS Science Computing Facility (SCF) to produce maps needed for 'quick-look' inspection of the Level 2 data.

Figure 2-1 shows an overview of the MLS Level 3 processing. The principal component of the Level 3 data processing to produce daily maps is the FFSM algorithm mentioned above and described later in section 3.1. The monthly map, and daily and monthly zonal means, will be produced by other algorithms discussed in section 3.2, 3.3, and 3.4. Inputs to the Level 3 processing are (1) the MLS Level 2 data and (2) a user input file which contains parameters that control the processing (see Appendix A).

The MLS Level 2 dataset is first interpolated to pre-set latitude grids. One grid has points at the latitudes that will be used for the Level 3 maps. The other is a grid at the nominal Level 2 latitudes, which is needed for producing zonal means at the full Level 2 latitude resolution. There are three processing steps from here: 1) daily maps on nominal Level 3 latitude and longitude grid; 2) monthly maps on nominal Level 3 latitude and longitude grid; and 3) daily and monthly zonal means at nominal Level 2 latitude. In all the processes, the entire aggregate of species (both dynamical and chemical), and vertical levels can be processed in parallel.

Before the FFSM is invoked, the Level 2 data in each latitude is `initialized`. This process includes sorting data into chronological order and into ascending and descending sequences, and data preprocessing (such as interpolation). The outputs from FFSM are Fourier coefficients of space and time for all products. The final step is to calculate the daily and monthly maps and zonal mean data, and output the results along with appropriate diagnostic information.

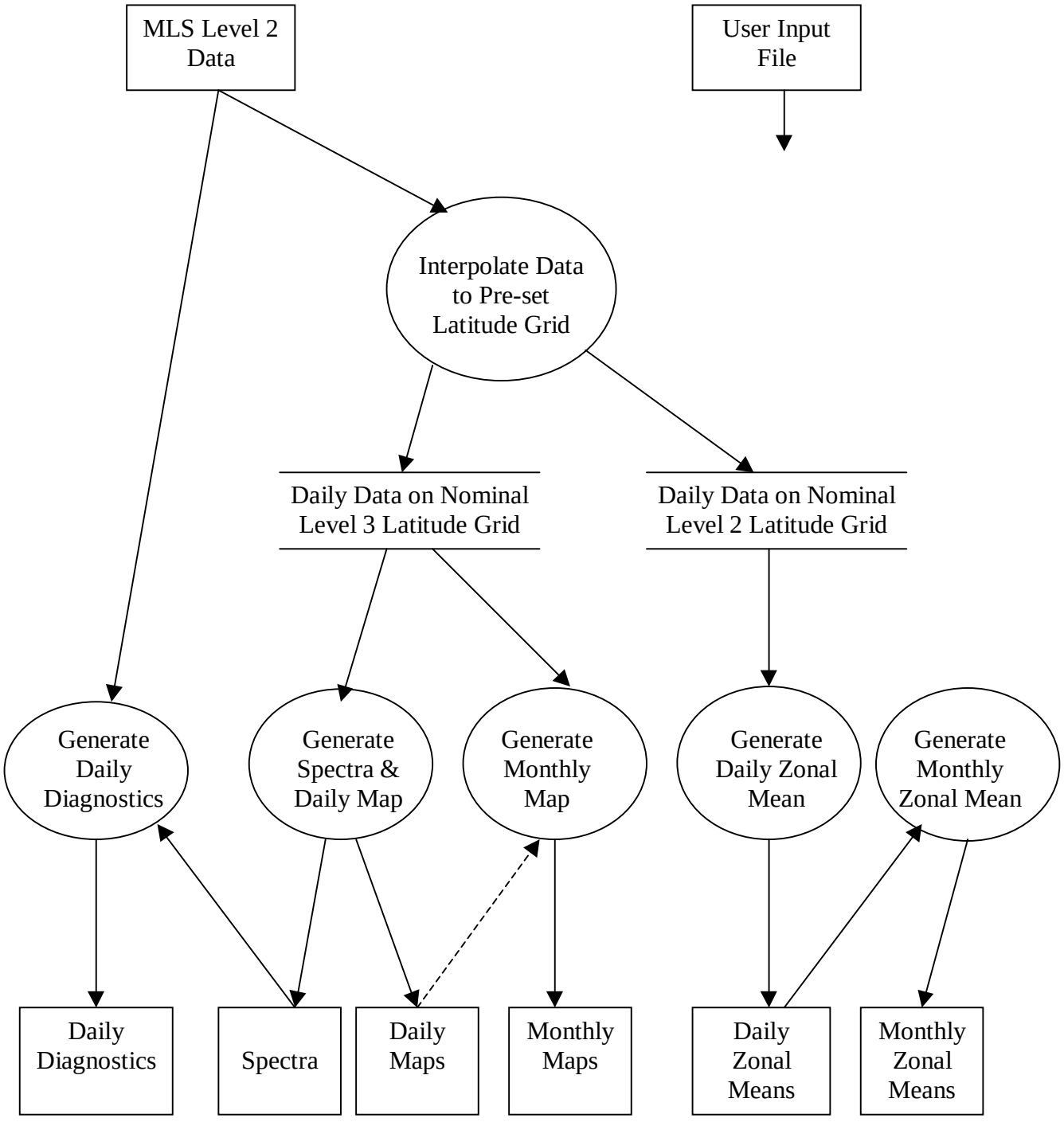

Figure 2-1. Overview of the EOS MLS Level 3 data processing for measurements with sufficiently high signal-to-noise to make daily/monthly synoptic maps and daily/monthly zonal mean, whose algorithms are described in this document.

3. EOS MLS Level 3 data processing algorithms

In this section, the details of the Fast Fourier Synoptic Mapping (FFSM) technique will be described. We will demonstrate the accuracy of the technique by using simple theoretical fields and real data respectively. We will also discuss the implementation and efficiency of the algorithm. Finally, some limitations of the technique will be presented.

3.1 Daily map products

3.1.1 Algorithms for converting Level 2 data to nominal latitude grids

As mentioned earlier in this document the EOS MLS Level 2 data are nominally produced every 1.5 degrees along the suborbital path. The Level 2 latitude spacing thus varies from approximately 1.5 degrees at the equator to only a few tenths of degree near the orbit 'turn around' points (near 82 degree latitude), as shown in Figure 3-1.

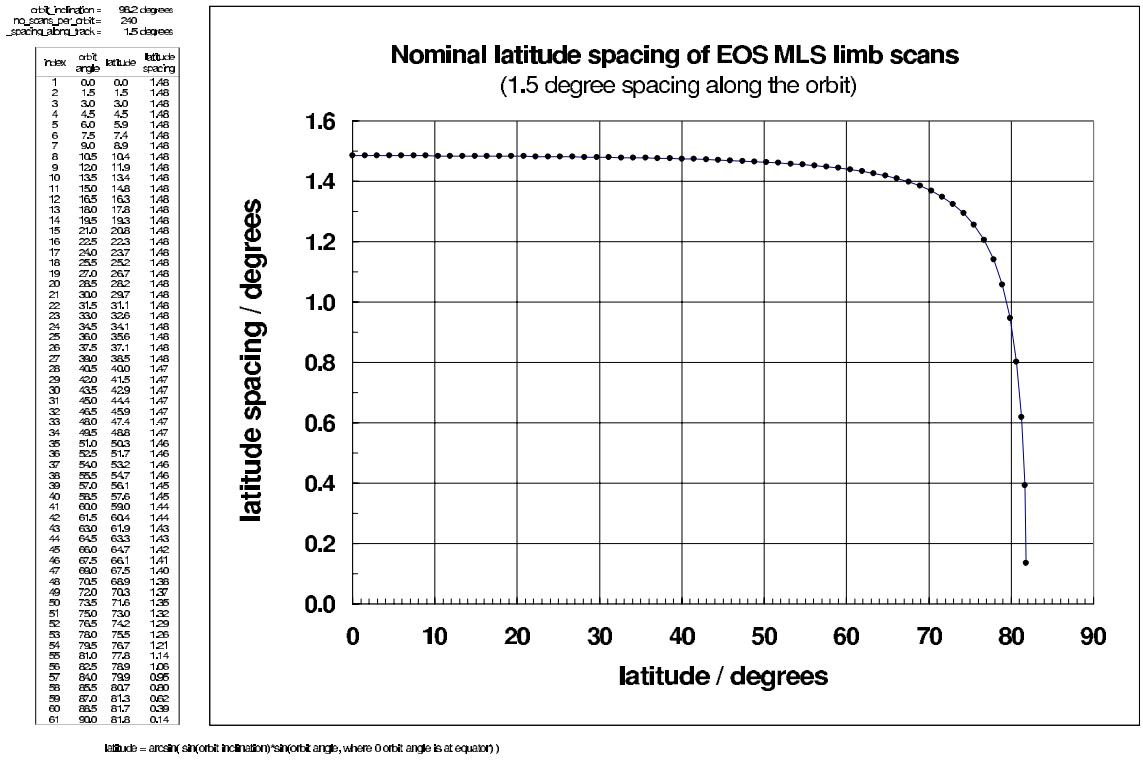

Figure 3-1. Latitude spacing between adjacent Level 2 data. Latitude of a measurement is related to the orbit angle α (defined as zero when measurement point is over the equator) by $\theta = \sin^{-1}\{\sin\beta \times \sin\alpha\}$, where β is the orbit inclination (98.2 degrees for EOS CHEM). Nominal latitudes for the EOS MLS Level 2 data are given in the third column of the table to the left of the plot.

The Level 2 data must be interpolated to the nominal latitudes (0, ±2, ±4, ... degrees) for the Level 3 maps, and also – for the zonal means – to the nominal Level 2 latitudes to account for any (expected small) differences between the actual and nominal Level 2 latitudes.

Missing or 'bad' Level 2 data must be 'filled in' in order to provide a continuous data set for use by the mapping algorithms described in section 3.1.2. Interpolating isolated missing points along the orbital track is straightforward by using linear or cubic spline fit method. But when a large gap exists in an orbit, however, interpolation along that orbit must be abandoned. Through numerical experimentation with transforms of artificial data and white noise, Lait and Stanford [1988] found that interpolation using a linear fit yields good results when the gap is larger, while cubic spline fit gives reasonable results when less than 5 points were missing. Therefore, the procedure dealing with missing data is to first interpolate missing data points along an orbit track. Then after data has been sorted into descending and ascending series at fixed latitudes, missing points in those series may be interpolated by linear or cubic spline which will avoid suppressing high frequencies in the small gaps and avoid unrealistic peaks in the large gaps.

The Level 2 data can also be interpolated to Level 3 nominal grids by using Fourier transform techniques along the track if the missing points have been filled in by using linear or cubic spline fit method. The 'along-track' spectra will likely prove useful for analyses of small scale structure seen in the data.

3.1.2 Algorithms for producing daily maps

3.1.2.1 Introduction

Two categories (asynchronous and geosynchronous) of orbital platforms have dominated Earth observations from space. Fixed with respect to the Earth, geosynchronous satellites observe a single region within their field of view all the time. Geostationary satellites provide measurements with higher temporal resolution than possible with asynchronous polar-orbiting satellites. However, geostationary satellites provide limited coverage and distortion at the limb of the field of view. For these reasons asynchronous satellites have been widely used for the monitoring of the Earth's atmosphere. Of these, polar-orbiting platforms (sun-synchronous in particular) are widely used today. An inherent advantage of this orbital geometry is nearly complete global coverage. High inclination orbits such as those of sun-synchronous satellites provide measurements nearly pole to pole, covering all longitudes in approximately a day, or in half a day when both dayside and nightside measurements can be made.

Although having advantages in coverage and vertical resolution, measurements taken from non-geosynchronous satellite are asynoptic. The asynoptic sampling results in different regions being observed at different times. Between the locations and times where measurements are taken, no information on the measured field's behavior is available. Because of these data voids, and that approximately a day passes before the full range of longitudes has been (perhaps sparsely) sampled, certain classes of behavior may escape observation.

The asynoptic nature of satellite measurements is especially important for variability that involves space and time scales comparable to those of the sampling. Fluctuations on small space and time scales are inherent to important components of the climate system. Undersampling of such behavior will lead to more gradual scales being aliased. Sampling properties are thus an important

aspect of satellite data. The discrete sampling in space and time is a key consideration that must be addressed in interpreting such observations.

A few approaches for estimating synoptic maps from asynoptic observations have been proposed. A full review of different techniques can be found in Salby [1982ab]. Currently, the most common, although crudest, analysis procedure is to interpolate the data in space and time by some means to a synpotic, regularly spaced grid. While adequate for examining slowly moving waves, such methods can introduce significant distortions of planetary scale waves with periods of 5 days or less [e.g. *Salby* 1982b]. Kalman filtering techniques (such as the sequential estimation method of Rodgers 1976) may be used to generate synoptic grids, but appropriately constructing the needed statistical models can prove troublesome.

Another method is by Chapman *et al*. [1974], in which soundings from ascending and descending orbit sequences at fixed latitudes are arranged in two time series and Fourier transformed. Peaks in the spectra correspond to one of many possible wavenumber-frequency pairs which are Doppler-shifted by the satellite's motion relative to the Earth to the same observed frequency F_0, given by

$$F_0 = m + sf$$

where m is the zonal wavenumber, f the frequency in cycles per day (cpd), and s = -1 for the westward-moving waves, s=+1 for the eastward-moving waves. This procedure suffers from an inherent ambiguity in ascribing a particular wavenumber and frequency from possible pairs of (m,f) to a spectral feature of F_0. Application of the asynoptic sampling theorem of Salby [1982a] narrows the number of allowed pairs to two, and by comparing the phase difference between the ascending and descending peaks one can usually determine which of the two is represented.

Of all of these techniques, the Fourier transform is most often used as a means of detecting periodic signals in data. A 2D transform isolates the periodicities that exist in two independent dimensions. The discrete zonal space-time Fourier transform of an observed data field $\psi(\lambda,t)$, sampled at regular intervals in λ and t, is given by

$$\Psi(k,\sigma) = \sum_{m=0}^{M-1} \sum_{n=0}^{N-1} \psi(\lambda_m, t_n) e^{-i(k\lambda_m + \sigma t_n)} \qquad (3.1)$$

where λ_m is the mth sampled longitude, t_n is the nth sampled time, k and σ are wavenumber and angular frequency (rad day^{-1}) respectively.

Because the asynoptic data position is a function of time, the above equation cannot be separated into two independent 1D FFTs. Also, all of the approaches dealing with asynoptic data require an understanding of the limitations posed by the sampling. These limitations associated with aliasing ambiguities are intrinsic to all discrete data.

Salby [1982a,b] developed a method for computing the exact space-time Fourier transform of asynoptic satellite data, as well as synoptic gridded fields from such transforms. It is shown via a rotation from synoptic to asynoptic coordinates, thus separating Eqn. (3.1) into two independent Fourier transforms, that the sampling pattern uniquely determines the space-time spectrum at all wavenumbers and frequencies within Nyquist limits. In this procedure, the spectral resolution and aliasing are well defined. Hayashi [1983] offered an alternative formulation of the technique, the "frequency transform method," which has been shown to be equivalent [*Salby and Hayashi*, 1985].

In this chapter, we will briefly review the theorem of Discrete Fourier Transform and aliasing problems, then details of Salby's method [*Salby,* 1982ab] are presented by establishing a unique correspondence between alias-free asynoptic data and synoptic maps. A procedure for retrieving the synoptic maps is then developed. Application of the method to EOS MLS data is then presented.

3.1.2.2 Discrete Fourier transform and aliasing

The Discrete Fourier Transform (DFT) is the most widely used method for determining the frequency spectra of digital signals. This is due to the development of an efficient algorithm for computing DFTs known as the Fast Fourier Transform (FFT). Before we get into Salby's method, we will first review the Discrete Fourier Transform theorem and sampling aliasing.

The discrete Fourier transform, $\psi(k)$, of an N-element, one-dimensional function, $\varphi(n)$, is defined as:

$$\Psi(k) = \frac{1}{N}\sum_{n=0}^{N-1}\varphi(n)e^{-i2\pi nk/N} \qquad (3.2)$$

The inverse transform is defined as:

$$\varphi(n) = \sum_{k=0}^{N-1}\Psi(k)e^{i2\pi nk/N} \qquad (3.3)$$

Just as the sampled data represents the value of a signal at discrete points in time, the result of a Fast Fourier Transform represents the spectrum of the signal at discrete frequencies. These discrete frequencies are a function of the frequency index k, the number of samples collected (N), and the sampling interval (Δt):

$$f(k) = \frac{k}{N\Delta t} \qquad (3.4)$$

where k = 0, 1, 2, ..., N-1. Thus, the frequency spectrum computed above ranges from 0 to $\frac{N-1}{N\Delta t}$. However, the frequencies associated with frequency indices greater than $N/2$ are above the *Nyquist frequency* (defined later) and are not physically meaningful for sampled signals. It is generally chosen to define the range of the frequency index k to be from ($-N/2$-1) to $N/2$ so that it is (nearly) centered around 0 frequency.

Resolution

The resolution is defined as $\frac{1}{N\Delta t}$. In the real world, only a limited range, T, of data points is considered when doing discrete Fourier transform. The consequence of the limited data range is in fact that a correct spectrum is impossible to obtain. Instead, convolution of the true spectrum with the finite range represents a certain smoothing of true spectrum. The degree of smoothing depends on the range T. A shorter T gives stronger smoothing. The spectrum thus calculated is therefore called the *averaged or weighted spectrum*.

The side-lobes of the frequency window can also lead to undesirable effects such as spectral leakage. Much effort has been made to eliminate windowing effect by modifying the weighting function applied to the data before the transform [*Båth,* 1974]. However, it is not possible to completely eliminate the windowing effect.

In summary, the main rules to follow when choosing the window length T are the following:

- A larger T will lead to more detail, i.e. to better resolution in the computed spectrum.
- A smaller T will lead to better stability or better reliability of the computed spectral, because the spectral smoothing then extends over a larger frequency interval.

One extreme, the infinite T, unattainable in practice, will lead to correct spectrum. The other extreme, a very small T approaching zero, will lead to a "*white spectrum*", no resolution at all. In an actual case, a compromise has to be made between various considerations (of resolution, stability, computer time economy, etc.) in the choice of an appropriate range T.

Aliasing

While the range T defines the fundamental period or the lowest frequency in the spectral analysis, the sampling interval Δt defines the highest resolvable frequency. Intuitively, we can understand that at least three points, i.e. two time-intervals ($2\Delta t$), are the minimum information needed to define one period. This means that the shortest period that can be detected is $2\Delta t$, or the highest resolvable frequency is $\frac{1}{2\Delta t}$. This frequency limit f_c for the calculated spectrum is referred to as the *Nyquist frequency* or *Nyquist limit*. Aliasing is a well-known phenomenon in sampled data analysis. It is a consequence of the fact that after sampling, every periodic signal at a frequency greater than the Nyquist limit looks exactly like some other periodic signal at a frequency less than the Nyquist limit (Figure 3-1). It occurs because the time function is not sampled at a sufficiently high rate, i.e., the sample interval Δt is too large. Therefore, if the function $\varphi(t)$ is not band-limited, i.e., $\psi(f) \neq 0$ for some $|f| > f_c$, then sampling will introduce aliasing. To prevent aliasing, frequency components above the Nyquist limit must be removed before sampling.

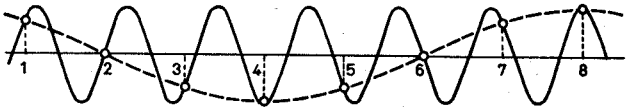

Figure 3-1. A well-known sketch demonstrating the effect of aliasing. By varying the sampling interval and the starting point, it is easily seen that different results will be obtained, regarding both amplitude, frequency and phase.

The rules for the frequency limits as caused by limited record length T and sampling interval Δt, can be summarized in the following rules:

- The record length T defines the lower frequency limit in the spectrum: $f_1 = \frac{1}{T}$.
- The sampling interval Δt defines the upper frequency limit in the spectrum: $f_N = \frac{1}{2\Delta t} = \frac{N}{2T}$, where N+1 is the number of data points. Contamination of computed spectra by frequencies higher than f_N is termed aliasing, sometimes spectrum folding.

Leakage

Leakage is related to having a non-integer multiple of the period in the data set. The effect of this is to create a periodic function with sharp *discontinuities*, as illustrated in Figure 3-2. Intuitively, we expect the introduction of these sharp changes in the time domain to result in additional frequency components in the frequency domain. In discrete Fourier transform, an N point record will produce an N point frequency response. Each of these points in the frequency response is called a frequency bin. Exactly where these frequency bins lie in terms of actual values depends on

the number of points in the record, as well as the sampling frequency. The more points, the closer the bins lie together, the higher the sampling frequency the further apart the bins are.

Figure 3-2 shows the example of sine wave that will suffer from spectral leakage with a range of 1.5 period. Since this is a pure sine wave, we would expect to see just one frequency at the frequency of the signal. However, since discrete Fourier transform assumes the signal to be periodic, the discontinuity at both ends of the signal will cause the leakage – the frequency of the signal won't be lying on any bin, it falls between the two bins closest to it. Therefore, the energy from the sample leaks out to the surrounding frequency bins (Fig. 3-3), and the magnitude of each of the samples is less than the magnitude of the ideal sample.

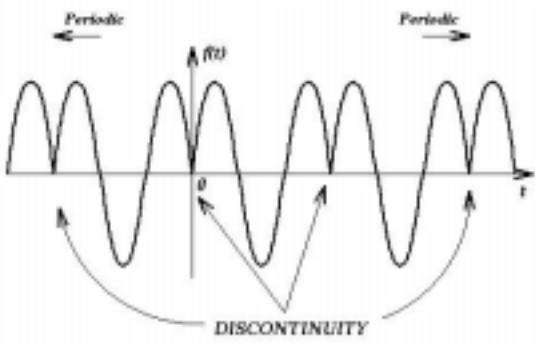

Figure 3-2. Sine wave with the discontinuity at the both ends.

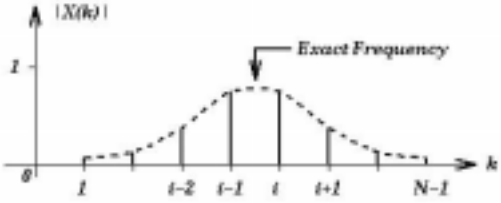

Figure 3-3. Spectra of the sine wave in Figure 3-2.

To complicate matters further, by increasing the number of samples to give greater resolution, the largest peak will get larger indicating it is nearer the true frequency. But the side samples where the energy has leaked to, will get larger as well and reduce the accuracy of the spectra.

3.1.2.3 Sampling geometry and coordinate rotation

EOS CHEM lies in a retrograde, near polar, orbit, defined by the orbital period τ_0 (98.8 min or 0.0686 day) and the angle of inclination 98.2^o from the equatorial plane. With τ_0 in units of days, a sun-synchronous satellite in such an orbit will complete

$$\nu_0 = \frac{1}{\tau_0}$$

orbits during one complete earth rotation (2π radians) and the satellite makes $2\nu_0$ ascending and descending measurements in one day on a given latitude circle.

Central to Salby's approach is the separation of measurements into ascending (northgoing) and descending (southgoing) series denoted here by subscripts *a* and *d*. Let c_0 be the angular velocity (radians/day) at which the orbital plane precesses along the latitude circle, so

$$c_0 = 2\pi$$

for sun-synchronous satellites. In the following discussion, we will consider a single latitude. Let λ_d and λ_a represent longitudes of descending and ascending measurements, respectively, for the latitude, with λ_{d0} and λ_{a0} their initial positions. Let t_d and t_a be the times at which the descending and ascending data are taken with t_{d0} and t_{a0} the initial times. Then we have

$$\begin{aligned} \lambda_{dj} &= \lambda_{d0} - c_0 \tau_0 j \\ \lambda_{aj} &= \lambda_{a0} - c_0 \tau_0 j \\ t_{dj} &= t_{d0} + \tau_0 j \\ t_{aj} &= t_{a0} + \tau_0 j \end{aligned} \qquad (3.5)$$

where j = 0, 1, 2, ..., N-1, and N is the total number of orbits used in the analysis.

The relationships between ascending and descending longitudes and times on any given latitude are the following (Fig. 3-4)

$$\begin{aligned} \lambda_{dj} &= \lambda_{aj} + \Delta\lambda_{ad} \\ t_{dj} &= t_{aj} + \Delta t_{ad} \\ \Delta\lambda'_{ad} &= \Delta\lambda_{ad} + c_0 \Delta t_{ad} \end{aligned} \qquad (3.6)$$

where $\Delta\lambda'_{ad}$ is the longitude separation between the loci of descending and ascending points along the line of constant time, which is also called the instantaneous separation. It would be the longitude separation as if descending and ascending observations are made simultaneously. Hence, $\Delta\lambda'_{ad} = \pi$ at the equator, but not at other latitudes.

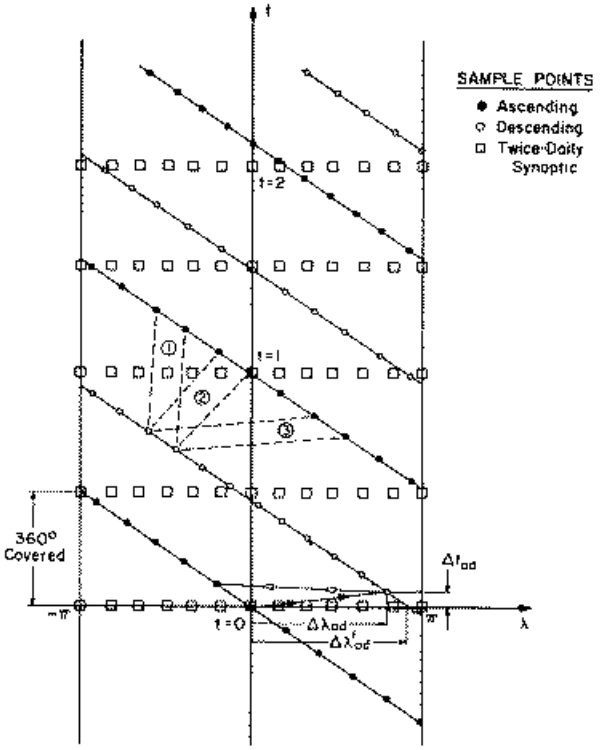

Figure 3-4. Sampling pattern of observations on a latitude circle in the longitude-time plane. The latitude circle is completely sampled by combined (ascending + descending) data in ½ day. Note ascending and descending trajectories are not equidistant. Twice-daily, synoptic sampling pattern also shown (adapted from Salby, 1982).

As shown by Salby [1982a], if we rotate synoptic coordinates (λ, t) by an angle α to the asynoptic coordinates (s, r) (Fig. 3-5b), where

$$\begin{aligned} \tan\alpha &= \frac{1}{c_0} \\ \sin\alpha &= \frac{1}{(1+c_0^2)^{\frac{1}{2}}} \\ \cos\alpha &= \frac{c_0}{(1+c_0^2)^{\frac{1}{2}}} \end{aligned} \qquad (3.7)$$

Then the relationships between synoptic and asynoptic coordinate systems are

$$\begin{aligned} \lambda &= s\cos\alpha + r\sin\alpha \\ t &= -s\sin\alpha + r\cos\alpha \end{aligned} \qquad (3.8)$$

$$\begin{aligned} s &= \lambda\cos\alpha - t\sin\alpha \\ r &= \lambda\sin\alpha + t\cos\alpha \end{aligned}$$

and

$$\begin{aligned} m &= k_s\cos\alpha + k_r\sin\alpha \\ \sigma &= -k_s\sin\alpha + k_r\cos\alpha \end{aligned} \qquad (3.9)$$

$$\begin{aligned} k_s &= m\cos\alpha - \sigma\sin\alpha \\ k_r &= m\sin\alpha + \sigma\cos\alpha \end{aligned}$$

Here k_s, k_r and m, σ are the wavenumbers and frequencies in asynoptic and synoptic coordinates respectively.

It follows that two contiguous nodes of either locus (Fig. 3-6) are separated by (See Appendix for derivation of these formulas)

$$\begin{aligned} \Delta s &= \frac{\tau_0}{\sin\alpha} \\ \Delta r_1 &= (2\pi - \Delta\lambda'_{ad})\sin\alpha \\ \Delta r_2 &= \Delta\lambda'_{ad}\sin\alpha \\ r_a &= \tfrac{1}{2}(\Delta r_1 - \Delta r_2) \\ r_d &= -\frac{R}{2} \\ \Delta\lambda'_{ad} &= (r_d - r_a)/\sin\alpha \end{aligned} \qquad (3.10)$$

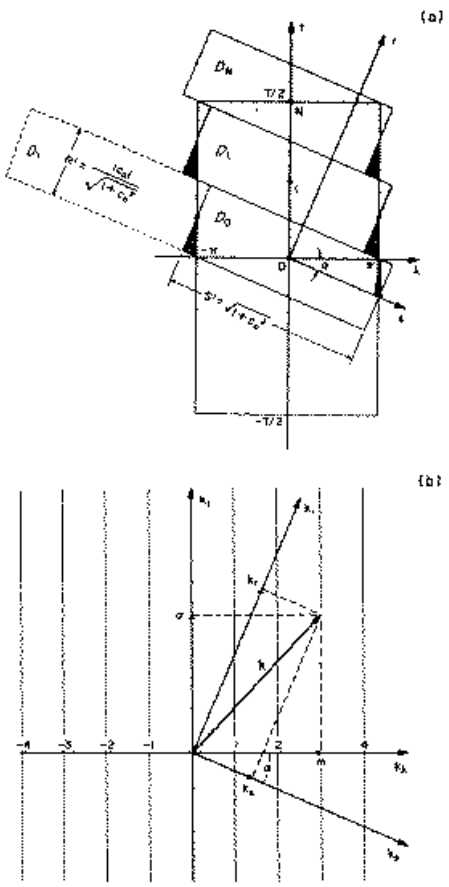

Figure 3-5. Coordinate geometry. (a) Physical plane: (*s*, *r*) coordinates are hybrids of longitude and time. Integration elements D_n do not perfectly cover the λ-t rectangle $D = [-\pi, \pi]\times[-T/2, T/2]$, but the miscoverage cancels in adjacent elements, leaving only the hyperextensions at $t = \pm T/2$. Because of zonal periodicity, each element D_n is equivalent to its periodic image; hence the integration may be performed over the strip of elements along the *s* axis. (b) Transform plane: k_λ, k_t, k_s, k_r are wavenumber components along respective axes (adapted from Salby, 1982).

3.1.2.4 Fast Fourier synoptic mapping

In reality, the Fourier transform must be calculated discretely. Synoptic sampling results in the choice of rectangles parallel to the (λ, t) axes as the integration elements (Fig 3-5). Therefore, in time region T (domain D in Fig 3-6), (3.1) becomes

$$\Psi(k,\sigma) = \frac{1}{2\pi T}\sum_{m=0}^{M-1}\sum_{n=0}^{N-1}\psi(\lambda_m, t_n)e^{-i(k\lambda_m+\sigma t_n)}\Delta\lambda\Delta t \qquad (3.11)$$

where

$$\Delta\lambda = \frac{2\pi}{M}$$
$$\Delta t = \frac{T}{N}$$

On the other hand, the 1-day integration element is defined in asynoptic coordinates (r, s) as a rectangle with sides of length (Fig 3-3)

$$R' = \cos\alpha$$
$$S' = \frac{1}{\sin\alpha}$$

Therefore, the integration can be performed for time region T over (r, s) strip $D' = [-S/2, S/2] \times [-R/2, R/2]$, where

$$R = R' = \cos\alpha$$
$$S = T \cdot S' = \frac{T}{\sin\alpha}$$

Here, D' is defined by locating the descending sequence at $r_d = -R/2$, and its periodic image at $R/2$. The ascending sequence lies somewhere (depending on the latitude) between these two (Fig. 3-3).

Then the Fourier transform in asynoptic coordinates (r, s) for the continuous case becomes

$$\Psi(k_s, k_r) = \tfrac{1}{RS}\int_{-R/2}^{R/2}\int_{-S/2}^{S/2}\psi(s,r)e^{-i(k_s s + k_r r)}dsdr$$

The discrete case becomes

$$\Psi(k_s, k_r) = \tfrac{1}{RS}\sum_{n=0}^{N}[\tfrac{1}{2}(\psi_{dn}e^{-i(k_s s_{dn} + k_r r_d)} + \psi_{an}e^{-i(k_s s_{an} + k_r r_{a)}})]\Delta r\Delta s + \mathrm{O}(\Delta s^2, \Delta r^2) \qquad (3.12)$$

where

$$\begin{aligned} s_{dn} &= -c_0\frac{\Delta r}{2} + n\Delta s \\ s_{an} &= s_{dn} - c_0\Delta r_2 + \frac{\Delta t_{ad}}{\sin\alpha} \\ \psi_{dn} &= \psi(s_{dn}, r_d) \\ \psi_{an} &= \psi(s_{an}, r_a) \\ T &= N\tau_0 \end{aligned} \qquad (3.13)$$

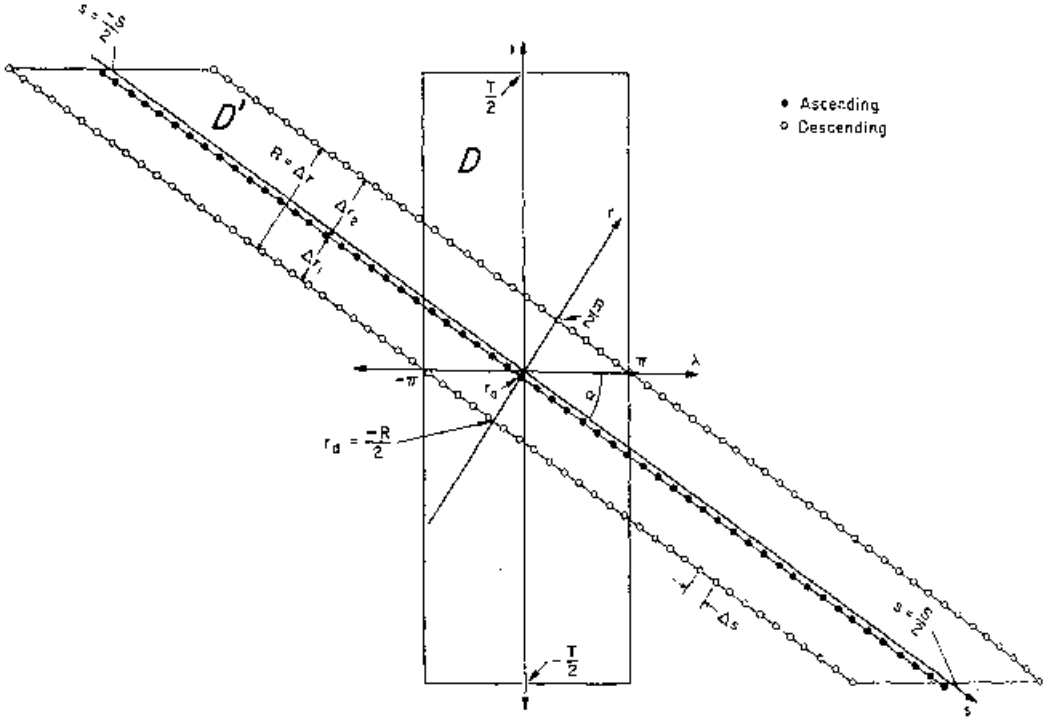

Figure 3-6. Synoptic *D*, and asynoptic *D'*, domains of transformation. The asynoptic strip is defined by the descending nodes located at *r=-R/2* and their periodic images at *r=R/2*. Ascending nodes lie at $r = r_a$, not in general equidistant, from the descending loci. Integration elements also shown (adapted from Salby, 1982).

(detail derivation of (3.13) can be found in the Appendix A)

The spectral resolutions along the k_s and k_r directions will be

$$\Delta k_s = \frac{2\pi}{S} = \frac{2\pi \sin\alpha}{T}$$
$$\Delta k_r = \frac{2\pi}{R} = \frac{2\pi}{\cos\alpha} \qquad (3.14)$$

and the Nyquist limits along the k_s and k_r directions are

$$k_s^N = \frac{\pi}{\Delta s} = \frac{\pi \sin\alpha}{\tau_0}$$
$$k_r^N = \frac{\pi}{\Delta r} \approx \frac{1}{\sin\alpha} \qquad (3.15)$$

The corresponding spectral resolution and Nyquist wavenumber along the m and σ directions in synoptic coordinates are (Fig. 3-7)

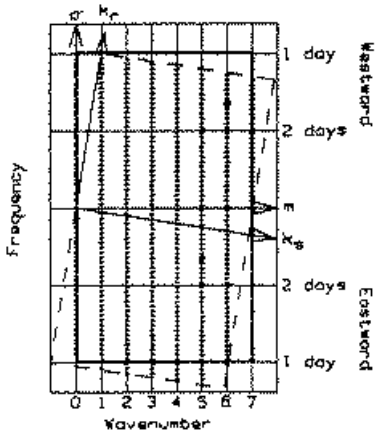

Figure 3-7. Location of points (tick marks) in the zonal space-time Fourier tranform of a 30-day series of asynoptic data. The dash lines mark the Nyquist limits as given by the FFSM technique, while the heavy lines indicate the Nyquist limits of a corresponding transform of synoptic data (adapted from Lait and Stanford, 1988).

$$\Delta m = \frac{2\pi}{S}$$
$$\Delta \sigma = \frac{2\pi}{T}$$
$$m^N = \frac{\pi}{\Delta\lambda}$$
$$\sigma^N = \frac{\pi}{\Delta t} \qquad (3.16)$$

The Nyquist limits in (m,σ) space correspond to a tilted rectangle, due to the rotation of coordinates as shown in Fig. 3-7. If we assume there are no spectral contributions from outside the Nyquist limits, it can be proved (section 3.1.2.4) that the space-time spectra $\Psi(k,\sigma)$ can be uniquely determined via the Fourier transform above. Therefore, the above theory also establishes the uniqueness between alias-free, asynoptic and synoptic sequences.

3.1.2.5 Explicit formulation of FFSM in *combined* mode

In the 2D Fourier Transform as given by Eqn. 3-12, there are only two terms, corresponding to ascending and descending, in the *r* direction in a period. Therefore, there are exactly 2 allowed "*r*" wavenumbers (k_r^- and k_r^+, defined later in Eqn. 3-22) for any given k_s inside the Nyquist rectangle $(-k_s^N, k_s^N)\times(-k_r^N, k_r^N)$ (Fig. 3-8). Thus, only two wave vectors, (k_s, k_r^-) and (k_s, k_r^+) on wavenumbers *m* and *m*+1, correspond to any value of k_s. This means that $\Psi(k_s, r)$ has a Fourier expansion in k_r containing only these two components. Therefore

$$\Psi(k_s, k_r) = \tfrac{1}{2}[\Psi(k_s, r_d)e^{-ik_r r_d} + \Psi(k_s, r_a)e^{-ik_r r_a}] \qquad (3.17)$$

where

$$\Psi(k_s, r) = \tfrac{1}{S}\sum_{n=-N}^{N}\gamma_n \psi(s, r)e^{-ik_s s_n}\Delta s \qquad (3.18)$$

As shown in Figure 3-8, k_r^- and k_r^+ can be derived to be

$$k_r^- = -k_s c_0 + m\sqrt{1+c_0^2}$$
$$k_r^+ = -k_s c_0 + (m+1)\sqrt{1+c_0^2} \qquad (3.19)$$

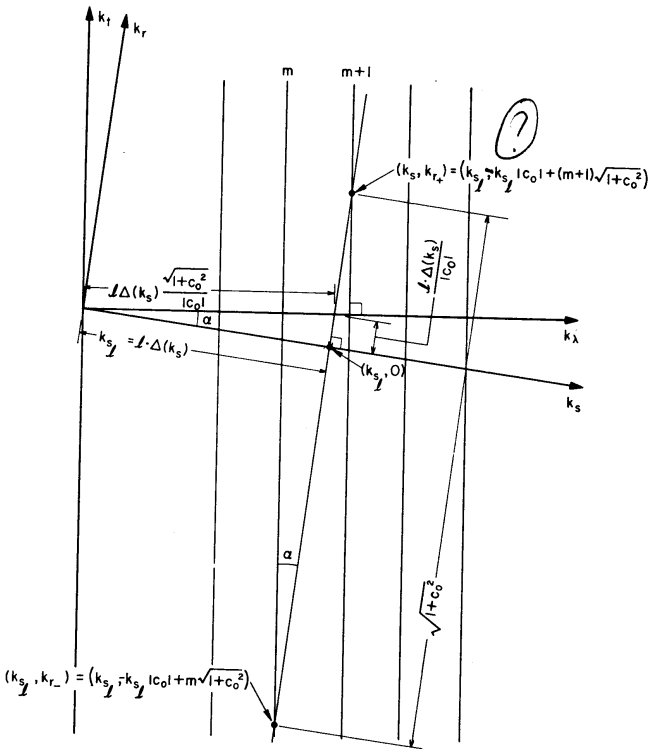

Figure 3-8. Construction of space-time spectra from transforms of asynoptic data. For each ks, there are two allowed spectra, corresponding to the points and on wavenumbers m and m+1, respectively (adapted from Salby, 1982b)

Since we know that $\Psi(k_s, r)$ contains exactly two Fourier components: $\Psi(k_s, k_r^-)$ and $\Psi(k_s, k_r^+)$, they are uniquely derivable from the two entities $\Psi(k_s, r_d)$ and $\Psi(k_s, r_a)$, provided the latter are independent. Then we have

$$\begin{aligned} \Psi(k_s, r_d) &= \Psi(k_s, k_r^-)e^{ik_r^- r_d} + \Psi(k_s, k_r^+)e^{ik_r^+ r_d} \\ \Psi(k_s, r_a) &= \Psi(k_s, k_r^-)e^{ik_r^- r_a} + \Psi(k_s, k_r^+)e^{ik_r^+ r_a} \end{aligned} \tag{3.20}$$

The solution is

$$\Psi(k_s, k_r^+) = \frac{\Psi(k_s, r_d)e^{-ik_r^- r_d} - \Psi(k_s, r_a)e^{-ik_r^- r_a}}{e^{i(k_r^+ - k_r^-)r_d} - e^{i(k_r^+ - k_r^-)r_a}}$$

$$\Psi(k_s, k_r^-) = \frac{\Psi(k_s, r_d)e^{-ik_r^+ r_d} - \Psi(k_s, r_a)e^{-ik_r^+ r_a}}{e^{-i(k_r^+ - k_r^-)r_d} - e^{-i(k_r^+ - k_r^-)r_a}}$$

This formula can be simplified to

$$\begin{aligned}\Psi(k_s,k_r^+) &= \frac{\Psi'(k_s,r_d)-\Psi'(k_s,r_a)}{e^{i\lambda_d}[1-e^{-i\Delta\lambda_{ad}^-}]}\\ \Psi(k_s,k_r^-) &= \frac{\Psi'(k_s,r_a)-\Psi'(k_s,r_d)e^{-i\Delta\lambda_{ad}'}}{1-e^{-i\Delta\lambda_{ad}'}}\end{aligned} \tag{3.21}$$

where

$$\begin{aligned}\Psi'(k_s,r) &= \Psi(k_s,r)\,e^{-i(k_s s_0+k_r r)}\\ k_r^- &= -k_s c_0 + \frac{m}{\sin\alpha}\\ k_r^+ &= -k_s c_0 + \frac{m+1}{\sin\alpha}\end{aligned} \tag{3.22}$$

(The derivation of formulas (3.20 and 3.21) is presented in Appendix A)

In order to avoid aliasing, k_r must satisfy $|k_r| \le 1/\sin\alpha$, so we have

$$\begin{aligned}-k_s c_0 + \frac{m}{\sin\alpha} &\ge -\frac{1}{\sin\alpha}\\ -k_s c_0 + \frac{m+1}{\sin\alpha} &\le \frac{1}{\sin\alpha}\end{aligned}$$

therefore

$$k_s\cos\alpha - 1 \le m \le k_s\cos\alpha \tag{3.23}$$

Because the transformed coordinate s decreases with time t, it is desirable to reverse the series. When this is done, the $N-1$ term becomes the first term of the series and must accounted for as an offset when performing the Fourier transform. Therefore we have

$$\begin{aligned}s_{d0} &= \lambda_{d0}\cos\alpha - t_{d0}\sin\alpha - \tau_0(N-1)/\sin\alpha\\ s_{a0} &= s_{d0} + (-c_0\Delta\lambda_{ad} + \Delta t_{ad})\sin\alpha\\ r_d &= (\lambda_{d0} + c_0 t_{d0})\sin\alpha\\ r_a &= (\lambda_{d0} - \Delta\lambda_{ad} + c_0 t_{d0} - c_0\Delta t_{ad})\sin\alpha\end{aligned} \tag{3.24}$$

Finally, we can get synoptic data by the following formula

$$\psi(\lambda_l,t_n) = \psi(s_l,r_n) = \sum_{|k_{s_j}|<k_{sN}}\ \sum_{k_r=k_r^{\pm}} \Psi(k_{s_j},k_r)\,e^{i(k_{s_j}s_l+k_r r_n)} \tag{3.25}$$

The formulas in this section are thus a generalization of the space-time transform for irregular asynoptic data. They constitute the Asynoptic Sampling Theorem which uniquely relates combined asynoptic data to their space-time spectrum. Thus, variability which involves only scales within the Nyquist rectangle (Fig. 3-7) can be unambiguously interpreted in asynoptic measurements. The

Asynoptic Sampling Theorem ensures that, if only such scales are present in a field being monitored, the variability is adequately sampled and the behavior can be recovered faithfully. However, if the field being monitored involves significant variance beyond the Nyquist limits, the behavior is undersampled. In such case, not only can the rapid variability beyond the sampling limits not be truly recovered, but more gradual scales within the Nyquist limits (which would otherwise be correctly retrieved) may be "aliased" or misrepresented because of these unresolved scales.

Sampling theory also provides a natural algorithm for synoptically mapping asynoptic measurements. Under the conditions of the Asynoptic Sampling Theorem (i.e., the field is adequately sampled), the full synoptic behavior can be recoved by inverting the space-time spectrum, derivable from the asynoptic measurements [*Salby* 1982b]. Fast Fourier Synoptic Mapping provides the actual sequence of synoptic maps, as if the measurements about the globe were taken simultaneously. Representing a unique transformation between asynoptic and synoptic coordinates, this scheme has been demonstrated as a generally reliable means of synoptically mapping asynoptic data [*Lait and Stanford* 1988a] and has allowed the identification of several rapidly propagating wave phenomena [*Lait and Stanford* 1988b].

3.1.2.6 Explicit formulation of FFSM in *single* mode

As mentioned before, some geophysical parameters may have strong diurnal variations. For these we will do the Fourier transform for ascending and descending series separately, because they generally represent local times separated by around 12 hours. There are exactly two terms, ascending and descending, in the *r* direction in a period in Fourier Transform as given by Eqn. 3-12. But for a single mode we only consider one series, ascending or descending. Therefore, the Nyquist limits of single mode along k_r direction become half of the combined mode and are given by

$$k_r^N = \frac{\pi}{2\Delta r} \approx \frac{1}{2\sin\alpha}$$

and the single mode Fourier Transform becomes

$$\Psi(k_s, k_r) = \Psi(k_s, r)e^{-ik_r r} \qquad (3.26)$$

where $\Psi(k_s, r)$ is defined in Eqn. (3-18).

As shown in Figure 3-8, k_r will be either $-k_s c_0 + m\sqrt{1+c_0^2}$ or $-k_s c_0 + (m+1)\sqrt{1+c_0^2}$ depending on which is in the Nyquist limits (but can not be both since the difference of these two is out of the Niquist limits).

Finally, we can get synoptic map for separate ascending and descending series by the following formula

$$\psi_a(\lambda_l, t_n) = \psi_a(s_l, r_n) = \sum_{|k_{s_j}|<k_{sN}} \Psi_a(k_{s_j}, k_r) e^{i(k_{s_j} s_l + k_r r_n)}$$
$$\psi_d(\lambda_l, t_n) = \psi_d(s_l, r_n) = \sum_{|k_{s_j}|<k_{sN}} \Psi_d(k_{s_j}, k_r) e^{i(k_{s_j} s_l + k_r r_n)} \quad (3.27)$$

Note that, the ascending and descending Fourier transform and reconstruction must be treated independently.

3.1.2.7 Procedure and data processing

The following summarizes the main processing steps for producing synoptic maps:

- Sort data into chronological order and into ascending and descending series respectively at each latitude, interpolate if necessary to cover bad or missing data
- Transform longitude and time in (λ,t) coordinates into (s,r) coordinates. Then perform FFT of ascending and descending nodes respectively
- Combine FFT of ascending and descending nodes for those fields which are not expected to have a significant diurnal signal
- Perform inverse FFT of combined spectra to produce synoptic maps of fields that are not expected to have significant diurnal signal, and also output the corresponding Fourier spectra
- Perform inverse FFT of ascending series, to produce day-side synoptic maps of the fields with diurnal variation, and also output the corresponding Fourier spectra
- Perform inverse FFT of descending series, to produce night-side synoptic maps of the fields with diurnal variation, and also output the corresponding Fourier spectra

These steps are illustrated in Figure 3-9.

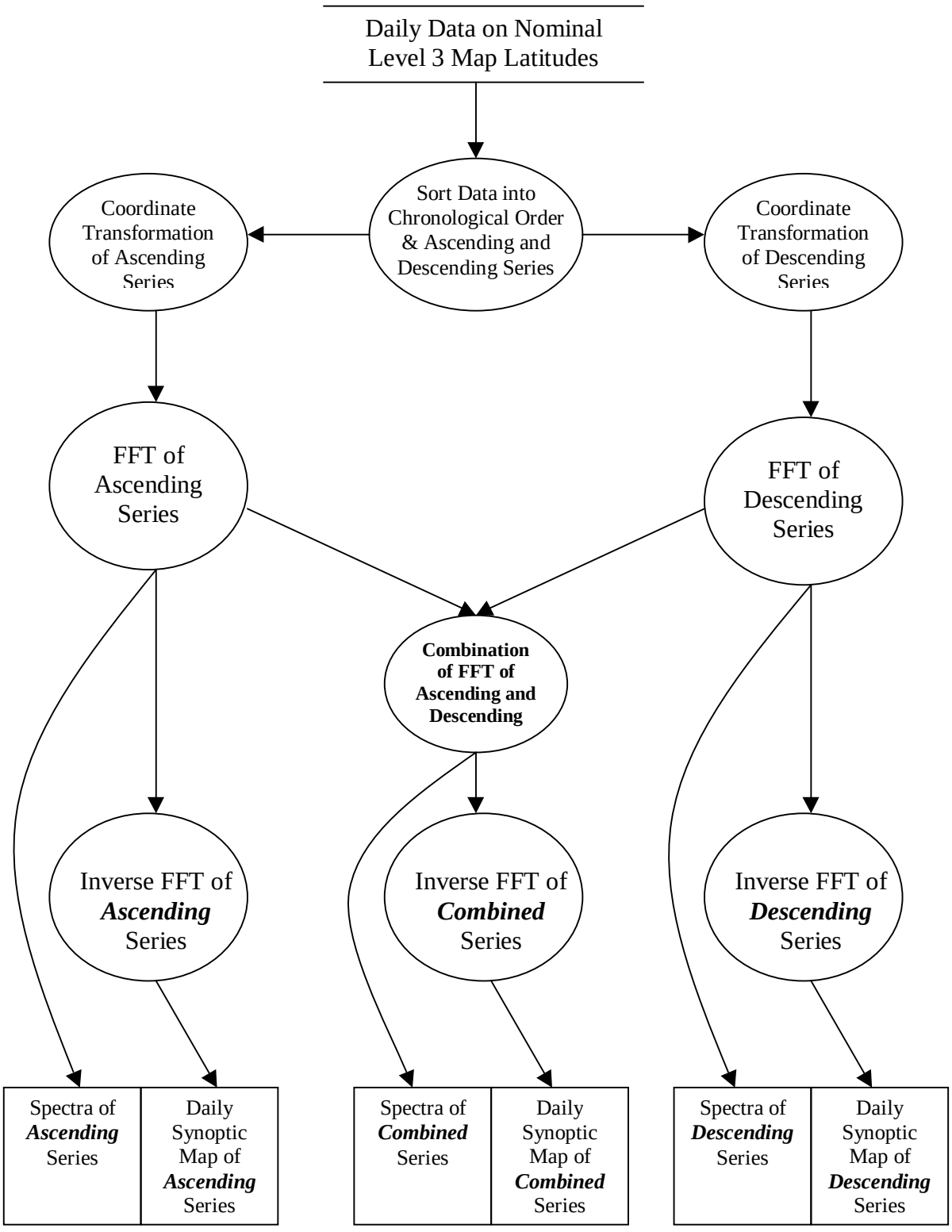

Fig. 3-9. Daily synoptic map generating procedure and data processing flowchart.

3.1.2.8 Issues and limitations

Spectra obtained by the asynoptic transform tend to become noisier towards the poles. As pointed out by Salby [1982a], as the satellite nears the meridional turning point of its orbit, the ascending latitude crossings approach the descending crossings. They coincide at the turning point (the most poleward latitude reached by the satellite). In terms of Figure 3-4, the ascending and descending lines become closer near the poles, thus the data field is greatly undersampled in some regions and oversampled in others along Salby's *r* direction, and the quality of the spectra deteriorates. In practice, this effect seems to be negligible equatorward of about 70^o-75^o latitude [*Lait and Stanford* 1988].

The asynoptic transform method, combining ascending and descending spectra, depends crucially upon the phase difference between the Fourier transforms of these two independent data series, each of which may contain irregular sampling, missing data, and nonstationary signals. But as shown by Salby [1982] and Lait and Stanford [1988], the FFSM technique is robust under both ideal conditions (such as exactly uniform data sampling intervals and no missing data) and typical real world conditions. The limitations of this technique must be kept in mind when interpreting the data. We now address some of the limitations.

a. *Aliasing*

A serious limitation of the FFSM technique is the aliasing that depends on the observing pattern and the signals present in the atmosphere. It is inherent in any analysis of the data, including the Kalman filter technique. Because EOS MLS covers the full longitude range twice (when combining ascending and descending sides of the orbits) in slightly less than 1 day, the Nyquist frequency corresponds to a period of 0.99 days and therefore variations with a period less than 0.99 days cannot be fully resolved. Variations with a period less than ~2 days cannot be fully resolved when using data separately from the ascending and descending portions of the orbits.

b. *Effects of satellite parameters and sampling errors*

The FFSM technique requires equal sampling intervals in both longitude and time, which is how the MLS Level 2 data will normally be produced. Sampling variations in both space and time may impair the accuracy of the spectra. Except for the changing orbital period of satellite as pointed out by Elson and Froidevaux [1993] for UARS, one may still interpolate to regular sampling points and then apply FFSM technique.

c. *Leakage, filtering and weighting*

The "smearing" or "leakage" effect of the Fourier Transform is a direct result of the definition of the Discrete Fourier Transform and is not due to any inaccuracy in the FFT. Leakage occurs when some of the actual frequency values do not lie in *frequency bins*. Therefore the energy of the actual spectrum leaks out to the surrounding frequency bins. Leakage can be reduced by increasing the length of the record, or by choosing a sample size that includes an integral number of cycles of the frequency component of interest, or by employing a windowing algorithm.

In the study of climate system such as the interaction between small-scale and high-frequency convection system in the tropical region, undersampled small-scale variability will aliases large-

scale variability which describes the organization of climate properties on space and time scale that would otherwise be correctly represented. Much of those undersampled variance in water vapor, cloud, and related distribution follows from small-scale convective structure, which comprises the convective pattern at any instant. Such structure involves space and time scales too short to be determined on a global basis from asynoptic data. However, the variance on those scales is largely random. Accordingly, the asynoptic power spectrum is dominated by broadband variance in a background spectrum that is (statistically) almost flat.

Salby and Sassi [1999] developed a scheme that utilizes the random nature of convective fluctuations to identify small-scale undersampled variance in asynoptic data and then eliminate it. Since random small-scale variations of a field are manifested in that field's complex amplitude spectrum by random phases of neighboring spectral components, processing the asynoptic spectrum with a convolution leads to a cancellation among incoherent spectral components. The scheme rejects a major component of undersampled convective variance, leaving a more accurate representation of large-scale variance. The prerequisite of this scheme is that the small-scale variability is random, therefore their phases are random. The scheme distinguishes itself when the power of broadband or background variance is comparable to the large-scale variations (low signal/noise ratio), such as in the tropical convective climate system. In the reconstruction of physical parameters from EOS CHEM satellite data, this scheme is useful to the retrieval of water vapor in the tropical region, and high noise parameters such as BrO. But its application to our reconstruction of synoptic map will definitely reduce the noise to certain levels.

3.1.2.9 Algorithm testing

There are several ways to test the FFSM scheme. By modeling the sampling pattern of satellite, we can test the scheme both analytically and realistically.

Simple tests using analytic functions as input from Salby [1982b] will be done to verify that signals inside the Nyquist limits are accurately represented.

More realistic tests involving the output of GCM simulations of the atmosphere will also be performed.

[Detail will be added later]

3.1.3 Diagnostics

Diagnostics and goodness-of-fit assessment will be produced as part of the retrieval of daily synoptic maps. The goodness-of-fit assessment summarizes the overall anomaly between the retrieved daily maps and the Level 2 data input to the algorithm. As shown in Figure 3-10, the Fourier spectra are used to construct the fields ϕ_i^r at the archived Level 2 latitudes (θ_i), longitudes (λ_i) and times (t_i) in one day period. Then an overall (global) `Level 3 residual` can be calculated as a root sum square (rss) difference

$$\sigma_{L3g} = \sqrt{\frac{1}{N}\sum_{i=1}^{N}(\phi_i^{\,r} - \phi_i^{\,m})^2} \qquad (3.28)$$

where ϕ_i^m is the measured field at (θ_i, λ_i, t_i).

In addition to rss σ_{L3g} as an overall evaluation of the retrieval, other diagnostics will be produced, such as:

Routine Diagnostics

- Maximum difference (maybe the first 10 or so largest) between the measured and reconstructed fields, and the location and time at which each occurred. This process will be separated between ascending and descending orbits (no overlapped points).
- The number or percentage of the missing points or the so-called "bad" data points from Level 2 analysis.
- Root sum square $\sigma_{L3DMP}(\varphi,p,\theta)$ for each latitude θ (separately for ascending & descending) for all geophysical parameters φ on selected pressure levels p. The plots of $\sigma_{L3DMP}(\varphi,p,\theta)$ as latitude on one page will be produced. The root sum square $\sigma_{L3DMP}(\varphi,p,\theta)$ is a good measure of high frequencies and wavenumbers that are outside the Nyquist limits. Furthermore, the comparison of $\sigma_{L3DMP}(\varphi,p,\theta)$ among some geophysical parameters will provide rich information on the chemistry and dynamics of the atmosphere.
- Error calculations
- Others ?

Special Diagnostics

- Daily anomaly map between constructed and measured fields. These maps will not be synoptic maps, but will be for the asynoptic measurement times in a day.
- Latitude variation of σ_{L3lat} in each latitude bin. User controls the latitude bin width.
- Confidence level of the retrieval
- Others ?

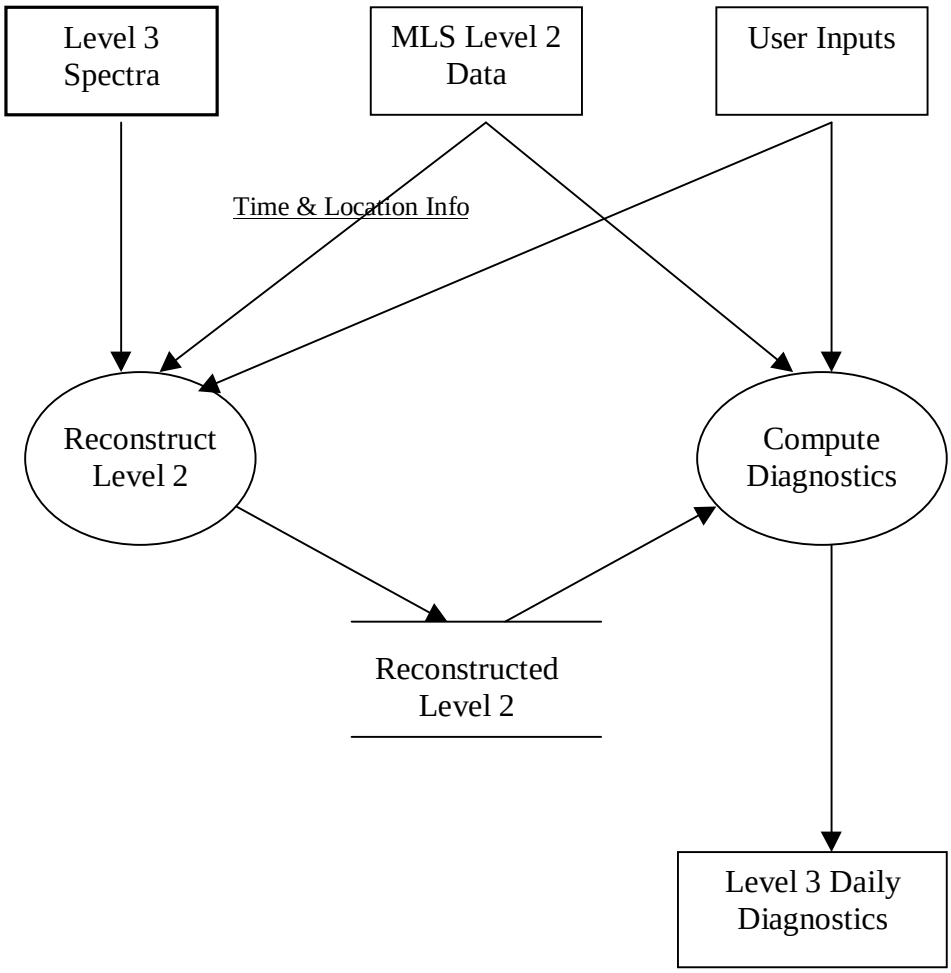

Figure 3-10. Generation of the EOS MLS Level 3 daily diagnostics.

3.2 Daily zonal mean products

3.2.1 Algorithms

Daily zonal mean products will be produced from the daily data on the nominal Level 2 latitude grid. The daily zonal mean at each latitude is obtained simply by averaging all the measurements in a day at that latitude. The software will have the capability, under the control of the user input file, to produce separate 'ascending-only', 'descending-only', and 'combined' zonal means.

3.2.2 Diagnostics

Daily zonal mean diagnostics being considered include:

- Standard deviation of points about the zonal mean σ_{L3DZM}.
- Flag the latitudes where daily zonal mean can not be obtained due to the lack of data.

3.3 Monthly map products

3.3.1 Algorithms

Monthly map products on the nominal Level 3 grid will be produced from the asynoptic daily data on nominal Level 3 grid. After interpolating MLS Level 2 data to nominal Level 3 Map grid as shown in Figure 2-1, the monthly maps will be obtained simply by averaging all the asynoptic daily data on nominal Level 3 grid in a month at each grid point.

3.3.2 Diagnostics

Monthly map diagnostics being considered include:

- Maps of the rss scatter of daily values about the monthly mean.
- Maps of the maximum and minimum daily difference from the monthly mean.

3.4 Monthly zonal mean products

3.4.1 Algorithms

Monthly zonal mean products on nominal Level 2 latitudes will be produced from the daily zonal means on nominal Level 2 latitudes. The monthly zonal means are obtained simply by averaging the daily zonal means for that month.

3.4.2 Diagnostics

Monthly zonal mean diagnostics being considered include:

- Standard deviation of points about the monthly zonal mean σ_{L3MZM}.

- Flag the latitudes where monthly zonal mean can not be obtained due to the lack of data.
- Flag the days when there are no data available.

4. Additional Topics

This section considers additional issues with MLS Level 3 data processing algorithms, including topics that, while not strictly part of the theoretical basis for the algorithms, are worthy of discussion here.

4.1 Tuning of algorithms and strategy for post-launch operations

Tuning of the algorithms includes the following:

- Choice of record range T
- Change of weighting function to be applied to the data before doing FFT
- Maximum size of missing data gaps
- Smoothing of spectra before reconstruction of synoptic maps
- others

[more to be added after results from V0.5 software]

4.2 Quality control, exception handling and related issues

4.2.1 Quality of products

In addition to produce synoptic maps for each physical parameters, the MLS data processing algorithms will compute an estimated uncertainty for each datum in the synoptic maps generated [algorithms to be provided later].

As described in section 3.1.3, the uncertainty on the generated result should always be compared with the uncertainty given in the input data. This comparison, along with the uncertainty information itself will form a major part of quality control. In the UARS MLS case, the uncertainty in Level 2 is set negative if it is greater than half of the *a priori* uncertainty. This serves as a useful flag to the users of the data, to indicate where and when data should be approached with caution. Similar flags may be implemented for EOS MLS Level 3, but these issues remain to be decided.

Another source of quality control information will be the σ_{L3g} information (see section 3.1.3). Cases where the retrieval of synoptic map is poor for some reason will be clearly indicated by a high value of σ_{L3g}. A complete set of σ_{L3g} statistics will be produced by the synoptic mapping algorithms routinely, giving the values of σ_{L3g} for each map generated. This σ_{L3g} information will also form the basis of a simple quality flag for each product, indicating the validity of the data, as was done for UARS MLS.

4.2.2 Bad or missing data

If the number of missing data does not exceed the limits that the algorithm can handle, the process of reconstruction of synoptic maps will continue. But the percentage of the missing points will be calculated and put in in diagnostics as pointed out in section 3.1.3.

4.2.3 Numerical exceptions

The synoptic mapping algorithm described here is sufficiently well posed and numerically stable that occurrences such as division by zero, or requesting the square root of a negative number should never occur. For this reason, no special handling is needed for such events; any attempt to perform such calculation will be indicative of a "bug" in the program, and so should simply bring the processing to an immediate halt with an appropriate error message.

4.3 Suitability of algorithms for modern computer architectures

The size of the EOS MLS data processing task is such that a parallel computer system will be required for the Level 3 synoptic mapping calculations. Since Level 3 synoptic mapping calculations of the entire aggregate of physical parameters, latitudes and vertical levels are independent, computations can be simultaneously parallel processed for the entire volume of observation. Thus, the Level 3 data processing is well suited to parallel computing. Clearly, the limitation here is the amount of data that can be simultaneously handled.

Perhaps the simplest parallel machine is a network of workstation type of computers; if these were the machines available, then one manner in which to perform the calculation would be to assign different pressure level of the dataset to a different processor. Clearly each computer would need a large amount of memory. An alternative to this approach is to divide the dataset into smaller groups of, say, five physical parameters over each pressure level, and distribute these among the available processors. The processors would then collaborate by performing all the calculations relevant to their elements of data, using message passing to communicate to their "neighbors" any components of the results they require for their calculations.

4.4 Computational requirements

To be added after results from prototype software are available.

4.5 Validation of Level 3 algorithms and data products

The approach to the validation of the EOS MLS data follows the procedure used successfully for the UARS MLS, and is summarized in the overview document [*Waters* 1999]. Some validation of the Level 3 algorithm itself will also be required. A vital tool for this validation is the use of GCM simulated atmosphere. Once a particular measurement pattern is known, the algorithm can be tested by sampling a known field from a GCM output. Comparison of synoptic maps with the original GCM output both in the presence and absence of instrumental noise and systematic errors yields valuable insight into the performance of the synoptic mapping algorithm. The primary validation of the Level 3 data will be the comparison of how well the reconstructed Level 2 field fits the actual Level 2 data.

4.6 Data volumes

Table 4.6-1 summarizes the estimated EOS MLS Level 3 routine daily data volumes. Values are given in terms of 'equivalent daily volume' (e.g., volumes for monthly files are divided by 30). Appendix B gives details on which these estimates are based.

Table 4.6-1. Level 3 Estimated Equivalent Daily Data Volumes.

Product name	equivalent volume for one day / Megabytes
Daily Map	28
Daily Map Diagnostics	13
Spectra	5
Monthly Map	1
Daily Zonal Means	0.3
Monthly Zonal Means	0.01
total	~50

Appendix A. User Input File Information

Information that has currently been identified for the Level 3 User Input File is itemized here. Many additional pieces of information are expected to be added as our concept for the Level 3 processing, and diagnostics, matures. It is also possible that, as part of the overall software design, it may be desirable to break the single "user input parameter file" implied in Figure 2-1 into several files (for example separate ones for daily and monthly maps, and daily and monthly zonal means).

1. Related to Level 2 Input Data

    - Which Level 2 data products are to be read
    - Which Level 2 data version to read
    - What range of days to input Level 2 data

2. Related to Output Data Products and Algorithm Control

    a. For interpolating to latitude grids:
        - Latitude grid for maps
        - Latitude grid for zonal means
        - What method(s) of interpolating Level 2 data for filling in missing or bad data
        - Maximum size of Level 2 data gap before Level 3 processing is halted
        - Whether 'along-track' spectra are to be computed and, if so, the parameters needed for controlling this computation

    b. For daily maps (following information to be provided separately for 'ascending-only', 'descending-only' and 'combined ascending/descending' maps):
        - The data products and pressure levels for which maps are to be produced
        - The range of wavenumbers and frequencies to be fit for each product
        - The range(s) of days to be used for fitting Fourier components for each product
        - The longitude grid for which mapped values are to be output for each product
        - The synoptic time for which mapped values are to be output for each product
        - The method(s) of low-pass filtering that are to be used before the Fourier transformation
        - The method(s) of weighting that are to be used after the Fourier transformation to reconstruct the synoptic maps
        - Information on diagnostic information to be produced, such as the following
            - Which, if any, data products, pressure levels, latitude ranges, and days for producing an anomaly file (difference between Level 2 data and values from Level 3 Fourier coefficients evaluated at time and location of each Level 2 measurement) and time-series.
            - The number N for the N largest differences between the Level 2 measurements and the Level 3 'reconstruction' of these measurements to output (the output file produced for this will include the values, differences, time, location, pressure, etc., for each – listed in decreasing absolute value of the difference)

- What data products, pressure levels, and days, for which a file is to be made of the latitude variation in zonal mean rss difference between Level 2 measurements and Level 3 reconstruction

c. For monthly maps (following information to be provided separately for 'ascending-only', 'descending-only' and 'combined ascending/descending' maps):
   - The data products and pressure levels for the maps that are to be produced
   - The method(s) of averaging to produce the 'monthly' map
   - The range(s) of days to be averaged together to produce the 'monthly' map
   - The version of Level 3 data to be used for producing these maps
   - Information on diagnostic information to be produced, such as the following
     - What products, if any, for producing a map of standard deviations of the daily data about the monthly mean
     - What products, if any, for producing a map of maximum deviations of the daily data about the monthly mean
     - What products, if any, for producing a map of data quality flags
     - ? What products, if any, for producing a map of number of data points that went into grid point for monthly map

d. For daily zonal means (following information to be provided separately for 'ascending-only', 'descending-only' and 'combined ascending/descending' zonal means):
   - The data products and pressure levels for the zonal means that are to be produced
   - Information on diagnostic information to be produced, such as the following:
     - What products, if any, for producing standard deviations of the individual points about the zonal mean
     - What products, if any, for producing maximum deviations of the individual points about the zonal mean
     - Whether to produce zonal mean and standard deviations of (1) the local solar time, (2) the local solar zenith angle, and (3) the line-of-sight angle at each latitude grid point

e. For monthly zonal means (following information to be provided separately for 'ascending-only', 'descending-only' and 'combined ascending/descending' maps):
   - The data products and pressure levels for the monthly zonal means that are to be produced
   - The range(s) of days to be averaged together to produce the 'monthly' zonal means
   - The version of Level 3 data to be used for producing these maps
   - Information on diagnostic information to be produced, such as the following:
     - What products, if any, for producing standard deviations of the daily data about the monthly mean
     - What products, if any, for producing maximum deviations of the daily data about the monthly mean
     - What products, if any, for producing a map of data quality flags
     - Whether to produce 'monthly' zonal mean and standard deviations of (1) the local solar time, (2) the local solar zenith angle, and (3) the line-of-sight angle at each latitude grid point

Appendix B. Data Volume Estimates

B.1 Output files of daily maps, diagnostics, and their FFSM spectra

Each file will contains only one standard geophysical data product and its diagnostics. These files will be used to examine the temporal evolution over many days of the maps for single parameters, and keeping the size of these files down to a few MB is worthwhile. The separate ascending and descending maps for the diurnally-varying parameters will be grouped together into the file for that data product. The daily map volume estimate is summarized in Table B.1-1.

Diagnostic information on the maps produced by Level 3 data processing will be put in the same files as the data. Some information planned for the daily map diagnostics is discussed in 3.1 and 3.2. The daily map diagnostic volume estimate is summarized in Table B.1-2.

FFSM spectra are produced separately for each standard geophysical data product. The spectra are produced from ~30 days of Level 2 data and used to reconstructed 10 days of daily maps. The ~30 days window used for producing the spectra will be moved forward 10 days for the next 10 days synoptic map reconstruction and so forth. Table B.1-3 gives the volume estimate for Level 3 FFSM spectra.

B.2 Output files of monthly maps

There will be one file (~30 MB) for each month which groups together monthly maps of all standard data products. The primary reason for grouping them together is to reduce the number of file names we have to keep up with. The monthly map volume estimate is summarized in Table B.2-1.

B.3 Output files of daily zonal means and monthly zonal means

Separate zonal means will be produced for the ascending and descending side of the orbits for all products, and will have the varying latitude resolution of Level 2 data. Files will contain both estimated value and precision for each datum that is produced.

A single file (~1 MB) will contain all zonal means of standard geophysical data products. One file for each day (daily zonal means), and one file for each month (monthly zonal means). This file will also contain zonal mean diagnostic information produced by Level 3 data processing. Some of the diagnostic information to be produced – for each latitude bin and each geophysical parameter – are discussed in 3.1 and 3.2. The volume estimates are shown in Table B.3-1 and Table B.3-2.

Table B.1-1. Level 3 Daily Map Products and Their Estimated Volumes. The number of pressure surfaces, and volumes, assume the maximum 12 retrieval points per decade pressure, and 4-byte words for the value and precision at each grid point.

Product name	Units	vertical range				number of pressure surfaces	volume for one day / Megabytes
		pressure / hPa		~ height / km			
		max	min	min	max		
TEMPERATURE	K	464	0.01	0	80	56	3.35
GEOPOTENTIAL_HT	Km	464	0.01	0	80	56	3.35
H2O	Vmr	464	0.01	0	80	56	3.35
HNO3	Vmr	100	1	15	50	24	1.43
O3	Vmr	316	.316	9	55	36	1.17
O3_ascending	Vmr	3.16	0.01	40	80	30	1,76
O3_descending	Vmr	3.16	0.01	40	80	30	1.76
HCl	Vmr	100	0.1	15	65	36	2.15
N2O	Vmr	215	1	9	50	28	1.67
ClO_ascending	Vmr	100	1	15	50	24	1.43
ClO_descending	Vmr	100	1	15	50	24	1.43
OH_ascending	Vmr	10	0.1	15	65	24	1.43
OH_descending	Vmr	10	0.1	15	65	24	1.43
HCN	Vmr	215	22	9	25	12	0.72
O3_STRAT_COLUMN	DU	Not applicable					0.06
						Estimated total daily volume	27.53

Table B.1-2. Level 3 Daily Map Products Diagnostics and Their Estimated Volumes. The number of pressure surfaces, and volumes, assume the maximum 12 retrieval points per decade pressure, and 4-byte words for the value and precision at each grid point.

Product name	units	vertical range				number of pressure surfaces	volume for one day / Megabytes	
		pressure / hPa		~ height / km				
		max	min	min	max		L3 residual	Others (TBD)
TEMPERATURE	K	464	0.01	0	80	56	1.61	
GEOPOTENTIAL_HT	km	464	0.01	0	80	56	1.61	
H2O	vmr	464	0.01	0	80	56	1.61	
HNO3	vmr	100	1	15	50	24	0.69	
O3	vmr	316	.316	9	55	36	1.04	
O3_ascending	vmr	3.16	0.01	40	80	30	0.86	
O3_descending	vmr	3.16	0.01	40	80	30	0.86	
HCl	vmr	100	0.1	15	65	36	1.04	
N2O	vmr	215	1	9	50	28	0.81	
ClO_ascending	vmr	100	1	15	50	24	0.69	
ClO_descending	vmr	100	1	15	50	24	0.69	
OH_ascending	vmr	10	0.1	15	65	24	0.69	
OH_descending	vmr	10	0.1	15	65	24	0.69	
HCN	vmr	215	22	9	25	12	0.35	
O3_STRAT_COLUMN	DU	not applicable					0	
						Estimated total daily volume	13.24	

Table B.1-3. Level 3 Spectra Products and Their Estimated Volumes. The number of pressure surfaces, and volumes, assume the indicated number of spectral output points per decade pressure, and 4-byte words for the value and precision at each grid point. Note that the spectra are not saved to the full vertical resolution of the maps or Level 2 data.

Product name	units	Vertical range				number of pressure surfaces per decade	volume for ~10 days period / Megabytes
		pressure / hPa		~ height / km			
		max	min	min	max		
TEMPERATURE	K	464	0.01	0	80	6	4.78
GEOPOTENTIAL_HT	km	464	0.01	0	80	6	4.78
H2O	vmr	464	0.01	0	80	6	4.78
HNO3	vmr	100	1	15	50	3	2.39
O3	vmr	316	.316	9	55	6	4.78
O3_ascending	vmr	3.16	0.01	40	80	3	2.39
O3_descending	vmr	3.16	0.01	40	80	3	2.39
HCl	vmr	100	0.1	15	65	3	2.39
N2O	vmr	215	1	9	50	6	4.78
ClO_ascending	vmr	100	1	15	50	3	2.39
ClO_descending	vmr	100	1	15	50	3	2.39
OH_ascending	vmr	10	0.1	15	65	3	2.39
OH_descending	vmr	10	0.1	15	65	3	2.39
HCN	vmr	215	22	9	25	3	2.39
O3_STRAT_COLUMN	DU	not applicable					0
Estimated total daily volume							47.80
Estimated equivalent total daily volume							4.78

Table B.2-1. Level 3 Monthly Map Products and Their Estimated Volumes. The number of pressure surfaces, and volumes, assume the maximum 12 retrieval points per decade pressure, and 4-byte words for the value and precision at each grid point.

product name	units	vertical range				number of pressure surfaces	volume for one month / Megabytes
		pressure / hPa		~ height / km			
		max	min	min	max		
TEMPERATURE	K	464	0.01	0	80	56	3.35
GEOPOTENTIAL_HT	km	464	0.01	0	80	56	3.35
H2O	vmr	464	0.01	0	80	56	3.35
HNO3	vmr	100	1	15	50	24	1.43
O3	vmr	316	.316	9	55	36	1.17
O3_ascending	vmr	3.16	0.01	40	80	30	1,76
O3_descending	vmr	3.16	0.01	40	80	30	1.76
HCl	vmr	100	0.1	15	65	36	2.15
N2O	vmr	215	1	9	50	28	1.67
ClO_ascending	vmr	100	1	15	50	24	1.43
ClO_descending	vmr	100	1	15	50	24	1.43
OH_ascending	vmr	10	0.1	15	65	24	1.43
OH_descending	vmr	10	0.1	15	65	24	1.43
HCN	vmr	215	22	9	25	12	0.72
O3_STRAT_COLUMN	DU	not applicable					0.06
Estimated total monthly volume							27.53
Estimated equivalent total daily volume							1.0

Table B.3-1. Level 3 Daily Zonal Means Products and Their Estimated Volumes. The number of pressure surfaces, and volumes, assume the maximum 12 retrieval points per decade pressure, and 4-byte words for the value and precision at each grid point.

product name	units	vertical range				number of pressure surfaces	volume for one day / Megabytes
		pressure / hPa		~ height / km			
		max	min	min	max		
TEMPERATURE	K	464	0.01	0	80	56	0.037
GEOPOTENTIAL_HT	km	464	0.01	0	80	56	0.037
H2O	vmr	464	0.01	0	80	56	0.037
HNO3	vmr	100	1	15	50	24	0.016
O3	vmr	316	.316	9	55	36	0.024
O3_ascending	vmr	3.16	0.01	40	80	30	0.020
O3_descending	vmr	3.16	0.01	40	80	30	0.020
HCl	vmr	100	0.1	15	65	36	0.024
N2O	vmr	215	1	9	50	28	0.019
ClO_ascending	vmr	100	1	15	50	24	0.016
ClO_descending	vmr	100	1	15	50	24	0.016
OH_ascending	vmr	10	0.1	15	65	24	0.016
OH_descending	vmr	10	0.1	15	65	24	0.016
HCN	vmr	215	22	9	25	12	0.008
O3_STRAT_COLUMN	DU	not applicable					0.000
Estimated total daily volume							0.314

Table B.3-2. Level 3 Monthly Zonal Means Products and Their Estimated Volumes. The number of pressure surfaces, and volumes, assume the maximum 12 retrieval points per decade pressure, and 4-byte words for the value and precision at each grid point.

product name	units	vertical range				number of pressure surfaces	volume for one month / Megabytes
		pressure / hPa		~ height / km			
		max	min	min	max		
TEMPERATURE	K	464	0.01	0	80	56	0.037
GEOPOTENTIAL_HT	km	464	0.01	0	80	56	0.037
H2O	vmr	464	0.01	0	80	56	0.037
HNO3	vmr	100	1	15	50	24	0.016
O3	vmr	316	.316	9	55	36	0.024
O3_ascending	vmr	3.16	0.01	40	80	30	0.020
O3_descending	vmr	3.16	0.01	40	80	30	0.020
HCl	vmr	100	0.1	15	65	36	0.024
N2O	vmr	215	1	9	50	28	0.019
ClO_ascending	vmr	100	1	15	50	24	0.016
ClO_descending	vmr	100	1	15	50	24	0.016
OH_ascending	vmr	10	0.1	15	65	24	0.016
OH_descending	vmr	10	0.1	15	65	24	0.016
HCN	vmr	215	22	9	25	12	0.008
O3_STRAT_COLUMN	DU	not applicable					0.000
Estimated total monthly volume							0.314
Estimated equivalent total daily volume							0.01

Appendix C. Derivation of Certain Formulae

C.1 Derivation of Eqn. (3-10)

From Fig.3-4, due to the rotation of asynoptic coordinates (r, s) relative to synoptic coordinates (λ, t), the separation Δs of two contiguous nodes of either locus is

$$\Delta s = \frac{\tau_0}{\sin\alpha}$$

Also we can immediately derive that

$$\Delta r_2 = \Delta\lambda'_{ad} \sin\alpha = \frac{\Delta\lambda'_{ad}}{(1+c_0^2)^{\frac{1}{2}}}$$
$$\Delta r_1 = (2\pi - \Delta\lambda'_{ad}) \sin\alpha = \frac{2\pi - \Delta\lambda'_{ad}}{(1+c_0^2)^{\frac{1}{2}}}$$

C.2 Derivation of Eqn. (3-13)

To derive equation

$$s_{dn} = -c_0 \frac{\Delta r}{2} + n\Delta s$$
$$s_{an} = s_{dn} - c_0\Delta r_2 + \Delta t_{ad}(1+c_0^2)^{\frac{1}{2}}$$

In Fig. 3-6 assuming the first descending point is at longitude $\lambda = 0$, then the corresponding coordinate in (r, s) is (from top descending loci in Fig 3-7)

$$s_{d0} = -c_0 \frac{\Delta r}{2}$$

therefore

$$s_{dn} = -c_0 \frac{\Delta r}{2} + n\Delta s$$

Now from

$$\Delta r_2 = \frac{\Delta\lambda'_{ad}}{(1+c_0^2)^{\frac{1}{2}}}$$

we have

$$\begin{aligned}\Delta\lambda'_{ad} &= \Delta r_2 (1+c_0^2)^{\frac{1}{2}} \\ \Delta\lambda_{ad} &= \Delta\lambda'_{ad} - c_0 \Delta t_{ad} \\ &= \Delta r_2 (1+c_0^2)^{\frac{1}{2}} - c_0 \Delta t_{ad}\end{aligned}$$

But from

$$s = \lambda \cos\alpha - t \sin\alpha$$

we have

$$\begin{aligned}s_a &= \lambda_a \cos\alpha - t_a \sin\alpha \\ &= (\lambda_d - \Delta\lambda_{ad})\cos\alpha - (t_d - \Delta t_{ad})\sin\alpha \\ &= s_d - \Delta\lambda_{ad}\cos\alpha + \Delta t_{ad}\sin\alpha \\ &= s_d - [\Delta r_2 (1+c_0^2)^{\frac{1}{2}} - c_0 \Delta t_{ad}]\cos\alpha + \Delta t_{ad}\sin\alpha \\ &= s_d - c_0 \Delta r_2 + \Delta t_{ad}(1+c_0^2)^{\frac{1}{2}}\end{aligned}$$

C.3 Derivation of Eqn. (3-21)

From (3.20)

$$\begin{aligned}\Psi(k_s, r_d) &= \Psi(k_s, k_r^-)e^{ik_r^- r_d} + \Psi(k_s, k_r^+)e^{ik_r^+ r_d} \\ \Psi(k_s, r_a) &= \Psi(k_s, k_r^-)e^{ik_r^- r_a} + \Psi(k_s, k_r^+)e^{ik_r^+ r_a}\end{aligned}$$

we can get

$$\begin{aligned}\Psi(k_s, k_r^+) &= \frac{\Psi(k_s, r_d)e^{-ik_r^- r_d} - \Psi(k_s, r_a)e^{-ik_r^- r_a}}{e^{i(k_r^+ - k_r^-)r_d} - e^{i(k_r^+ - k_r^-)r_a}} \\ \Psi(k_s, k_r^-) &= \frac{\Psi(k_s, r_d)e^{-ik_r^+ r_d} - \Psi(k_s, r_a)e^{-ik_r^+ r_a}}{e^{-i(k_r^+ - k_r^-)r_d} - e^{-i(k_r^+ - k_r^-)r_a}}\end{aligned}$$

Let's first simplify $\Psi(k_s, k_r^-)$:

$$\begin{aligned}\Psi(k_s, k_r^-) &= \frac{\Psi(k_s, r_a)e^{-ik_r^+ r_a} - \Psi(k_s, r_d)e^{-ik_r^+ r_d}}{e^{-i(k_r^+ - k_r^-)r_a} - e^{-i(k_r^+ - k_r^-)r_d}} \\ &= \frac{\Psi(k_s, r_a)e^{-ik_r^+ r_a}e^{-ik_r^- r_a}e^{ik_r^+ r_a} - \Psi(k_s, r_d)e^{-ik_r^+ r_d}e^{-ik_r^- r_a}e^{ik_r^+ r_a}}{e^{-i(k_r^+ - k_r^-)r_a}e^{-ik_r^- r_a}e^{ik_r^+ r_a} - e^{-i(k_r^+ - k_r^-)r_d}e^{-ik_r^- r_a}e^{ik_r^+ r_a}} \\ &= \frac{\Psi(k_s, r_a)e^{-ik_r^- r_a} - \Psi(k_s, r_d)e^{-ik_r^- r_d}e^{ik_r^- r_d}e^{-ik_r^+ r_d}e^{-ik_r^- r_a}e^{ik_r^+ r_a}}{e^{-i(k_r^+ - k_r^-)r_a}e^{-ik_r^- r_a}e^{ik_r^+ r_a} - e^{-i(k_r^+ - k_r^-)r_d}e^{-ik_r^- r_a}e^{ik_r^+ r_a}}\end{aligned}$$

By using $\Psi'(k_s, r) = \Psi(k_s, r)e^{-i(k_s s_0 + k_r r)}$, the above formula can be simplified to

$$\Psi(k_s, k_r^-) = \frac{\Psi'(k_s, r_a) - \Psi'(k_s, r_d) e^{-i(k_r^+ - k_r^-)(r_d - r_a)}}{1 - e^{-i(k_r^+ - k_r^-)(r_d - r_a)}}$$

From (3.10) and (3.22), we get

$$k_r^+ - k_r^- = 1/\sin\alpha$$
$$\Delta\lambda'_{ad} = (r_d - r_a)/\sin\alpha$$

Finally the derived equation becomes

$$\Psi(k_s, k_r^-) = \frac{\Psi'(k_s, r_a) - \Psi'(k_s, r_d) e^{-i(r_d - r_a)/\sin\alpha}}{1 - e^{-i(r_d - r_a)/\sin\alpha}} = \frac{\Psi'(k_s, r_a) - \Psi'(k_s, r_d) e^{-i\Delta\lambda'_{ad}}}{1 - e^{-i\Delta\lambda'_{ad}}}$$

Now let's simplify $\Psi(k_s, k_r^+)$:

$$\Psi(k_s, k_r^+) = \frac{\Psi(k_s, r_d) e^{-ik_r^- r_d} - \Psi(k_s, r_a) e^{-ik_r^- r_a}}{e^{i(k_r^+ - k_r^-) r_d} - e^{i(k_r^+ - k_r^-) r_a}}$$
$$= \frac{\Psi'(k_s, r_d) - \Psi'(k_s, r_a)}{e^{i(k_r^+ - k_r^-) r_d}\left[1 - e^{-i(k_r^+ - k_r^-)(r_d - r_a)}\right]}$$
$$= \frac{\Psi'(k_s, r_d) - \Psi'(k_s, r_a)}{e^{ir_d/\sin\alpha}\left[1 - e^{-i\Delta\lambda'_{ad}\sin\alpha/\sin\alpha}\right]}$$
$$= \frac{\Psi'(k_s, r_d) - \Psi'(k_s, r_a)}{e^{i\lambda_d}\left[1 - e^{-i\Delta\lambda'_{ad}}\right]}$$

C.4 Derivation of Eqn. (3-22)

In (k_s, k_r) space, for each k_s, there are two allowed spectra, corresponding to the points (k_s, k_r^-) and (k_s, k_r^+) on wavenumbers *m* and *m*+1, respectively. From (3.9), we can get

$$\sigma = \frac{m\cos\alpha - k_s}{\sin\alpha}$$

Substitute into (3.9) again, we have

$$
\begin{aligned}
k_r^- &= m\sin\alpha + \frac{m\cos\alpha - k_s}{\sin\alpha}\cos\alpha \\
&= -k_s\frac{\cos\alpha}{\sin\alpha} + \frac{m}{\sin\alpha} \\
&= -k_s c_0 + \frac{m}{\sin\alpha}
\end{aligned}
$$

We can get

$$k_r^+ = -k_s c_0 + \frac{m+1}{\sin\alpha}$$

by the same procedure.

Appendix D. Examples of results from prototype software

[To be added later]

Appendix E. Others to be added as needed

REFERENCES

Båth, M., 'Spectral Analysis in Geophysics,' *Elsevier*, Amsterdam, p95, 1974.

Brigham, O. E., 'The fast Fourier transform and its applications,' *Prentice Hall*., Englewood Cliffs, New Jersey 07632, 1988.

Canziani, P. O., J. R. Holton, E. Fishbein, L. Froidevaux, and J. W. Waters, 'Equatorial Waves: A UARS MLS view,' *J. Atmos. Sci.*, **51**, 3053, 1994.

Chapman, W. A., M. J. Cross, D. A. Flower, G. E. Peckham and S. D. Smith, 'A Spectral analysis of global atmospheric temperature fields observed by the selective chopper radiometer on the Nimbus 4 satellite during the year 1970-1,' *Proc. Roy. Soc. London*, A, **338**, 57, 1974.

Elson, L. S., and L. Froidevaux, 'Use of fourier transforms for asynoptic mapping: Application to the Upper Atmosphere Research Satellite Microwave Limb Sounder,' J. Geophys. Res., **98**, 23039, 1993.

Hayashi, Y., 'Modified methods of estimating space-time spectra from polar-orbiting satellite data. Part I: The frequency transform method,' *J. Meteor. Soc. Japan*., **98**, 23039, 1993.

Jarnot, R.F., 'EOS MLS Level 1 Data Processing Algorithm Theoretical Basis,' Jet Propulsion Laboratory Document D-15210**,** Version 1.0, dated 15 October 1999.

Lait, L. R. and J. L. Stanford, 'Applications of asynoptic space-time Fourier Transform Methods to scanning satellite measurements,' *J. Atmos. Sci*., **45**, 3784, 1988.

Livesey, N.J., and D.L. Wu, 'EOS MLS Retrieval Processes Algorithm Theoretical Basis,' JPL Document D-156159, Version 1.1 dated 15 October 1999. (available on the MLS web site, http://mls.jpl.nasa.gov)

Salby, M.L., 'Sampling theory for asynoptic satellite observations. Part I: Space-time spectra, resolution and aliasing,' *J. Atmos. Sci*. **39**, 2577, 1982a.

Salby, M.L., 'Sampling theory for asynoptic satellite observations. Part I: Fast Fourier synoptic mapping,' *J. Atmos. Sci*. **39**, 2601, 1982b.

Salby, M.L., and F. Sassi, 'Synoptic mapping of convective structure from undersampled satellite observations,' 1999 (in review).

Waters, J.W., 'An Overview of the EOS MLS Experiment,' JPL Document D-15745, Version 1.1 dated 15 October 1999. (available on the MLS web site, http://mls.jpl.nasa.gov)